Calhoun
Institutional Archive of the Naval Postgraduate School

Calhoun: The NPS Institutional Archive

DSpace Repository

Theses and Dissertations 1. Thesis and Dissertation Collection, all items

1998

Electromagnetic launchers for use in aircraft launch at sea

Still, Aaron Michael.

Monterey California. Naval Postgraduate School

http://hdl.handle.net/10945/8301

This publication is a work of the U.S. Government as defined in Title 17, United States Code, Section 101. Copyright protection is not available for this work in the United States.

Downloaded from NPS Archive: Calhoun

DUDLEY KNOX LIBRARY

Calhoun is the Naval Postgraduate School's public access digital repository for research materials and institutional publications created by the NPS community. Calhoun is named for Professor of Mathematics Guy K. Calhoun, NPS's first appointed -- and published -- scholarly author.

Dudley Knox Library / Naval Postgraduate School
411 Dyer Road / 1 University Circle
Monterey, California USA 93943

http://www.nps.edu/library

NPS ARCHIVE
1998.05
STILL, A.

DUDLEY KNOX LIBRARY
NAVAL POSTGRADUATE SCHOOL
MONTEREY CA 93943-5101

Electromagnetic Launchers for Use in Aircraft Launch at Sea

by

Aaron Michael Still, B.S.S.E.

Thesis

Presented to the Faculty of the Graduate School of
The University of Texas at Austin
in Partial Fulfillment
of the Requirements
for the Degree of

Master of Science in Engineering

The University of Texas at Austin
May 1998

PS Archive
98.05
till, A.

~~253~~
c.

DUDLEY KNOX LIBRARY
NAVAL POSTGRADUATE SCHOOL
MONTEREY CA 93943-5101

Electromagnetic Launchers for Use in Aircraft Launch at Sea

Approved by
Supervising Committee:

____

____

Acknowledgements

The author would like to thank his adviser, Dr. Mircea D. Driga, for all of his guidance and the in-depth knowledge that allowed for the completion of this thesis. Also, the author would like thank Dr. Martin L. Baughman for his help and comments. Also, the author would like to thank Mr. Raymond C. Zaworka, Jr. of the Center for Electromagnetics at the University of Texas at Austin for his expert advice and assistance. Finally, the author would like to thank Mr. Joseph A. Gandell for his technical assistance.

Aaron M. Still

The University of Texas
May 1998

Abstract

Electromagnetic Launchers for Use in Aircraft Launch at Sea

by

Aaron Michael Still, M.S.E.
The University of Texas at Austin, 1998
Supervisor: Mircea D. Driga

The purpose of this thesis is to investigate the feasibility of an electromagnetic launcher for aircraft launch at sea. To accomplish this task, the performance requirements and physical constraints for an aircraft launcher were determined. Also, a review of previously used aircraft catapult was completed. In addition to this, an investigation into previously designed electromagnetic launchers was done. A review of electromagnetic launcher theory is also necessary. An investigation of different power systems was done. Finally, experimentation into the practical use of electromagnetic launchers must be done. All of this investigation led to the conclusion that the coilgun type of electromagnetic launchers meets all of the requirements to be used to launch aircraft at sea.

Table of Contents

List of Figures vii

SECTION I: INTRODUCTION **10**

Chapter 1: The Need for an Electromagnetic Aircraft Launcher 11

Chapter 2: Requirements of an Electromagnetic Aircraft Launch 14

SECTION II: PREVIOUSLY DESIGNED AIRCRAFT LAUNCHERS **16**

Chapter 3: The History of Aircraft Launchers 17

Chapter 4: The Flush Deck Catapult 24

Chapter 5: The Steam Catapult 26

Chapter 6: The Electropult 32

Chapter 7: The 1970's Electromagnetic Launcher Design 37

Chapter 8: Kaman's Electromagnetic Aircraft Launcher 45

SECTION III: THEORY OF LINEAR INDUCTION LAUNCHER **55**

Chapter 9: The Railgun and the Coilgun 56

Chapter 10: Stresses on Electromagnetic Launchers 68

Chapter 11: Idealized Model of a Coilgun 72

Chapter 12: The Limits of the Coilgun 81

Chapter 13: Scaling Factors for Linear Induction Launchers 97

Chapter 14: Transitions in a Multi-Section Launcher 105

Chapter 15: Conclusions of Electromagnetic Theory 120

SECTION IV: POWER SYSTEMS **122**
Chapter 16: Pulsed Power Systems 123
Chapter 17: Pulse Forming Networks 128
SECTION V: THE ELECTROMAGNETIC GUN EXPERIMENT **138**
Chapter 18: Electromagnetic Gun Diagnostic Theory 139
Chapter 19: Electromagnetic Gun Experimentation 145
SECTION VI: CONCLUSIONS **152**
Chapter 20: Overall Conclusions 153
Chapter 21: Thought for Improvements in Electromagnetic Launchers 155
APPENDIX A: CVX REQUIREMENTS FOR THE 21ST CENTURY **160**
REFERENCES **166**
Vita 172

List of Figures

Figure 1: The Progression of the Catapult with Respect to Delivered Energy 23
Figure 2: Steam Catapult Force Profile 29
Figure 3: Diagram of the Steam Catapult 31
Figure 4: Short stator (a) and short rotor (b) linear machines. 33
Figure 5: Schematic of the Electropult 34
Figure 6: Photograph of the Electropult Prototype 36
Figure 7: Three Phase Coaxial Accelerator 39
Figure 8: Schematic of the EMC electric power system 42
Figure 9: Artist's conception of the EMC 43
Figure 10: Enlarged view of the catapult shuttle 44
Figure 11: Diagram of a Disk Alternator 46
Figure 12: Diagram of the Launch Motor 50
Figure 13: EMAL Force Profile 52
Figure 14: The basic diagram of a railgun. 58
Figure 15: The basic geometry of a coilgun. 63
Figure 16: Polyphase barrel with sleeve projectile 73
Figure 17: Planar sheet model of coilgun 74
Figure 19: Filamentary coaxial coils 82
Figure 20: Thin pancake coils 84

Figure 21: Armature coil with finite length ... 85
Figure 22: Stator coil and armature excitation ... 86
Figure 23: Coordinate System ... 108
Figure 24: Elementary Volumes ... 109
Figure 25: Elementary conductive volumes ... 110
Figure 26: Electric branch of the equivalent network ... 112
Figure 27: Two section linear induction launcher ... 115
Figure 28: Velocity profile for different values of the initial position in the second section ... 117
Figure 29: Velocity profile for different values of the initial position in the second section ... 118
Figure 30: Required Trapezoidal Current Pulse ... 129
Figure 31: Lossless L-C ladder network. ... 130
Figure 32: Auxiliary Parallel Network ... 130
Figure 33: Complete L-C Ladder Network ... 134
Figure 34: Schematic drawing of plasma-armature railgun ... 139
Figure 36: Geometry of the gun rails and the diagnostic coil ... 146
Figure 37: Predicted B-dot voltage for the BTR tests ... 144
Figure 38: Current waveforms for 10 shots using ceramic sidewalls and Inconel 718 rails in the BTR. ... 148
Figure 39: B-dot 1 waveforms for 10 shots using ceramic sidewalls and Inconel 718 rails in the BTR. ... 149

Figure 40: B-dot 2 waveforms for 10 shots using ceramic sidewalls and Inconel 718 rails in the BTR. 150

Figure 41: Pressure transducer #2 waveforms for ten shots using ceramic sidewalls and Inconel 718 rails in the BTR. 151

SECTION I: INTRODUCTION

The purpose of this thesis is to investigate the feasibility of an electromagnetic launcher for aircraft launch at sea. To accomplish this task, the performance requirements and physical constraints for an aircraft launcher must be determined. Also, a review of previously used aircraft catapult must be completed. In addition to this, an investigation into previously designed electromagnetic launchers must be done. A review of electromagnetic launcher theory is also necessary. Along with the theory, an investigation of different power systems must be completed. Finally, experimentation into the practical use of electromagnetic launchers must be done.

Chapter 1: The Need for an Electromagnetic Aircraft Launcher

With the 21st century on the immediate horizon, the United States Navy has many modernization issues that need to be addressed to meet its ever-changing strategic goals. The missions and threats of the next century are not very apparent. The lack of a specific area of concern does allow the United States Navy to address three areas of known concern.

The first of these issues is to convert the focus of the Navy from a large global threat by a powerful nation or group of nations (e.g. the Soviet Union and the Warsaw Pact) to smaller region threats from a variety of foes. The later of these threats is referred to as low-intensity conflict. In order to prepare for low-intensity conflicts, the Navy's platforms must be able to perform a variety of missions both independently and within groups.

Another area of concern that the Navy must address is efficiency. In the era of the Cold War, the efficiency of a system was secondary to its reliability and its performance. The adage "if it ain't broke, don't fix it" would accurately describe the goals of the era. In the age of decreasing defense budgets, the priority of efficiency will join reliability and performance as equals. Quick inspections of many naval vessels will show modern systems next to systems that are decades out of date.

Unfortunately, the older systems are not only inefficient in regards to their intended purpose but also inefficient in their use of space. More compact systems with higher efficiency would require less manpower to both operate and maintain. This fact is very significant because the crew is one of the most expensive components of the ship. By designing new systems that are more efficient, more compact and require a smaller crew, the volume and weight of ships can be decreased thus making the overall system more efficient.

The final area of concern for the Navy of the 21st century is maintaining its technological superiority over its potential foes. In fact, this final concern should be all of the incentive required for modernization of the fleet.

From these three areas of concern, the Navy can focus their efforts in many directions. One such direction could be to design new systems that continue the advancement of technology without a decrease in productivity. Another direction could be to develop more efficient systems to replace older systems that waste precious resources such as space, weight, energy and manpower. A third direction could be to replace existing systems with newer ones that have more flexibility.

The current system for aircraft launch at sea is one system where all of these goals can be achieved. By replacing the current steam catapults with an

electromagnetic launcher, the Navy can have a more efficient system in regards to weight and volume. Also, the electromagnetic launchers will waste less of the ship's power. These more advanced systems will require less manpower to operate and maintain. Finally, the electromagnetic launchers will be capable of use for a variety of aircraft.

with a variation of 0 to 1.5 m/s, a cycle time of 45 seconds, and a maximum peak-to-mean tow force ratio of 1.05. One of the more important requirements of a new launch system will be to increase the system's energy efficiency without reducing its reliability. Lastly, the new system could not be nearly as maintenance intensive as the current system (Doyle, 528).

SECTION II: PREVIOUSLY DESIGNED AIRCRAFT LAUNCHERS

This section contains a review of the various aircraft launchers that have been either used or designed. Chapter 3 consists of an overall history of the aircraft catapult. Chapter 4 is an expanded explanation of the flush deck catapult. The current steam catapult is discussed in depth in Chapter 5. Chapter 6 is a discussion of the original electromagnetic launcher called the Electropult. Chapter 7 is a review of a design for an electromagnetic launcher that was proposed in the 1970’s. Finally, Chapter 8 discusses a design for an electromagnetic aircraft launcher from the 1990’s.

Chapter 3: The History of Aircraft Launchers

Ever since the airplane was first dreamed, man has thought of ways to get their airplanes into the air. To meet this need, the catapult has played an important role in the development of airplanes. During the early attempts by the Wright Brothers at flight, the power of gravity was used to assist their takeoff. By sliding down a sand dune while being guided by a railroad junction, gravity brought the plane up to speed at which the engines were able to take over. In the same era, Dr. Samuel Langley was working on a more powerful and complex method for launching a manned aircraft to be able to fly under its own power. While its was extremely well funded, Langley's catapult failed miserably (Jablonski, 53-4).

When the Wright Brothers moved their operation inland and away from the sloped sand dunes on the beaches in 1904, they followed Langley's lead by designing and constructing a catapult launcher of their own. Because of their lack of funds, the Wright Brothers took a more pragmatic approach to their launching mechanism. While Langley's failed design was based on a spring mechanism, the Wright Brothers again used the power of gravity. The gravity catapult that they designed obtained its motive power from the inertia of the falling weight, rope, and pulley apparatus that was

attached to the front of their airplane. When the weight was released, the kinetic energy of the falling weight was transferred to the aircraft by means of the rope and pulley system. This force dragged the plane up to speed and into the air in a much shorter distance than their previous design of the railroad junction (Miller, 199).

As the viability of flight was becoming proven in early parts of the 20th century, the military became interested in the uses of aircraft. During World War I, the military used the new technology of aircraft for reconnaissance and some minor bombing ("The Steam Catapult" 14). Seeing these military applications for aircraft, the United States Navy took an interest in the use of aircraft in modern naval warfare. While a majority of the Navy's admiralty envisioned the use of naval aircraft in a similar manner to that used in World War I (i.e. scouting, minor bombing), some others (e.g. Admiral William Sims and Brigadier General William Mitchell) envisioned flying squadrons of aircraft that would make the traditional battleship obsolete (Miller, 199).

With the uses for aircraft in naval warfare still either undecided or unknown, the U.S. Navy began research into ship-based aircraft. After devising a method to land planes onboard ships known as aircraft carriers, The Navy and many independent entrepreneurs began a massive research and development program to find the most effective way to launch the planes from ships. It should be noted that a

ship with a runway that is long enough for the aircraft to take off on their own would be too long for practical use. After a failed initial test in the summer of 1912, a catapult powered by compressed air was successfully tested in November 1912 and was able to be fitted on the larger ship in the fleet including battleships (United States, 14).

The compressed air catapult worked in similar manner to the Wright Brothers' gravity catapult with the falling weight being replaced by compressed air. The piston that held the compressed air has a stroke of 40 inches and was designed to bring the plane to takeoff speed gradually. Attaching the plane to the compressed air rig required a cable that was wound through the series of pulleys and was fixed to the piston at one end and the shuttle at the other. The aircraft was held to the shuttle by a retractable metal fitting that was tripped at the front of the catapult. When the piston was fired, the cable pulled the plane along a 30-foot long launching rail built on top of the large gun turrets and into the air (Skerrett, 512).

With the development of the compressed air catapult, a mobile fleet of aircraft was becoming a reality for the U.S. Navy. During the years between the world wars, more research took place yielding six more experimental catapults. Finally, an ideal catapult for the earlier carrier was created known as the flush deck catapult. Despite its positive attributes, the flush deck catapult

was becoming outdated during the war (United States, 17-18). As World War II intensified, the planes became heavier from an increase in armors and weapons. This substantial increase in the weight of the planes being launched from aircraft carriers, the development of a more powerful compressed air catapult was needed. To fulfil this need, a new form of the flush deck catapult was fitted on the carrier on the Navy fleet. This new flush deck catapult was 96 feet long that was capable of launching an 18,000 lbs. aircraft at 79 knots. A companion catapult was also installed that was capable of propelling a 16,000-lbs. aircraft into the air at 72 knots in a space of 72.5 feet (United States, 16-17). While these new catapults were able to meet the need of the Navy fleet during World War II, it became obvious that the invention of jetpower would make the flush deck catapult obsolete in the near future.

Because of the growing need for a more powerful aircraft launching system, engineers pursued two new areas of catapult power: electromagnetic and steam. In the mid-1940's, the Westinghouse Corporation began work on an aircraft launcher that drew its power from electromagnetics. In 1946, a prototype of this launcher was built for testing. This new launcher known as the Electropult. The Electropult produced a thrust of 50kN at a speed of 60 m/s for a power output of 3 MW but only at an overall efficiency of significantly less than 50%. While sound in theory, the Electropult proved to be an

unsuccessful attempt to replace the flush deck catapult. A more detailed look appears in another section (Laithwaite, 153-155).

The other power source that was being considered to be use in the replacement of the flush deck catapult was steam. The majority of the work done with a steam-powered catapult was done in Great Britain following World War II. In 1950, the British Royal Navy devised a revolutionary method to create the necessary power to propel the massive jets and planes from the deck of the contemporary aircraft carriers. This new design was known as the Steam Catapult. The U.S. Navy quickly tested and adopted the steam catapult in 1954 for use aboard its aircraft carriers. The design adopted in 1954 has undergone only a few minor improvements and is still in use today (United States, 26).

Though the 1950's and 1960's, the Navy seemed content with the performance of the steam catapult. In the 1970's, the Navy began to explore new avenues in aircraft launchers. With the developments of linear motors in high-speed ground transportation, the Navy began inquiries into similar technologies for aircraft catapults. These new electromagnetic launchers promised higher efficiency and thrust rates with lower weight and volume. In their efforts to explore the electromagnetic launcher, the Navy received proposals from many research laboratories. The most interesting of the designs was submitted by the Center for Electromechanics at the University of Texas at Austin.

Their approach was a linear asynchronous motor without sliding contacts. This design promised to be the most feasible replacement for the steam catapult; however, the navy never followed through with their investigation leaving the electromagnetic aircraft catapult on the drawing board (Weldon, 1-2). More of this design will follow in another section.

It was not until the 1990's that the Navy rekindled their interest in replacing the steam catapult. With shrinking budgets and advances in power electronics, the Navy relieved that the electromagnetic launcher offered enough benefits to explore. As a result, the Naval Air Warfare Center and Kaman Electromagnetics began a study into the electromagnetic aircraft launcher. This study concluded with the design of a linear synchronous motor with a power system of four disk alternators and a cycloconverter (Doyle, 528-529). A further investigation of this continuing study follows in another section.

With the new research into electromagnetic launchers, the history of the aircraft catapult appears to be adding a new chapter. From the Wright Brothers' gravity launcher to the flush deck catapult and the steam catapult, the changes in assisted aircraft take-off seems to progress at a parallel rate as that of the aircraft.

Figure 1: The Progression of the Catapult with Respect to Delivered Energy (Doyle, 532)

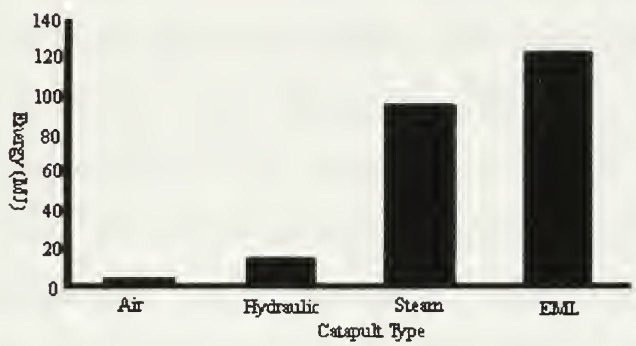

Chapter 4: The Flush Deck Catapult

In 1935, it was concluded through experimentation that a compressed air catapult provided the most effective means of launching aircraft from ships at sea. It was also found that this compressed air catapult could be installed beneath the deck of the aircraft carrier. The name given to this compressed air catapult was the flush deck catapult. In a space of only 34 feet, the flush deck catapult was capable of launching a 5,500-lbs. aircraft at 39 knots (United States, 13).

In order to change the current compressed air catapult into the new flush deck catapult, only one major change was needed. In place of the retractable metal fitting that secured the plane to the catapult shuttle, a metal cable known as the bridle was attached to the aircraft. Then the bridle was looped around the spreader which is a metal finger that protruded from the shuttle beneath the deck. When the catapult was fired, the shuttle dragged the plane by the bridle along the deck of the carrier and into the air.

There was no comparison between the flush deck catapult and the older methods of launching aircraft from ship that included the turret-mounted catapult and simply driving the planes off the deck. The most important feature of the flush deck catapult was that it required

very little space on the deck. This allowed the carrier to have more planes on the deck at any one time. Another important feature of the flush deck catapult was that it made launches more controllable. This was especially true in rough seas. Also, the flush deck catapult made it possible to precisely time the launches with the rocking of the boat. This task was difficult and extremely dangerous during an unassisted launch. Also, the flush deck catapult decreased the need for lighting aboard the deck of the carrier. The flush deck catapult allowed pilot to take off "blind". This was important because it did not make pilots rely on dim lighting for take-off that decreased accidents. Perhaps more importantly, with fewer lights aboard the carriers were less likely to be seen or accurately targeted by enemy ships (United States, 20-22).

The flush deck catapult performed a very commendable job during the early parts of World War II. During the later parts of the war, the flush deck catapult needed to be upgraded to handle the heavier aircraft being used. The upgrade increased the length by 38.5 feet to 72.5 feet (Steam, 16-17).

Chapter 5: The Steam Catapult

The United States Navy has been investigating the possibility of replacing the existing steam catapults on current aircraft carriers with electromagnetic launchers (Doyle, 528). The current C13-1 steam catapult is a burden on the ship's power plant. Among the reported disadvantages of the C13-1 are its excessive weight, its dependency on the ship's central steam plant, its volume, the large amounts of fresh water consumption, and maintenance difficulties (Weldon, 1).

The steam catapult is approaching its operational limit with the current and future complements of the carrier airwing. There has been a trend to build heavier, faster aircraft that will results in a launch energy requirement that exceeds the capability of the steam catapult (Doyle, 528). Also, the steam catapult is not flexible enough to decrease the amount of launch energy is provides making the steam catapult incapable of assisting the short takeoff and landing aircraft (STOL) currently used by the U.S. Marine Corps.

The existing steam catapults located on U.S. Navy aircraft carriers consist of two parallel rows of slotted cylinders in a trough 1.07m deep, 1.42 m wide, and 101.68 m long. The steam catapult is located directly below the flight deck (Doyle, 528).

As the name implies, the steam catapult is powered by high-pressure steam. The steam is used to drive the two pistons through long metal tubes called power cylinders. Each piston is able to maintain steam pressure behind itself and simultaneously allows itself to be fixed to the shuttle that tows the aircraft between the power cylinders.

This is accomplished by a part of the piston called the connector that has two functions. The first function of the connector is to connect the piston to the shuttle by means of branching out of the top of the power cylinders. The second function of the connector is to manipulate the sealing strip. The sealing strip is a flexible strip of metal that runs the entire length of each power cylinder. When steam pressure is introduced into the power cylinders, the sealing strips are forced against the opening in the top flange of the power cylinder. Therefore, it is necessary for the connector to both unseat the sealing strip and reseat it to maintain pressure in the cylinders as the piston moves. The bearing pad and the guide perform the unseating and reseating of the sealing strip. The former displaces it while the later resets it. To provide a means of attaching the aircraft to the pistons, the wheeled shuttle is linked to the connector assembly and then secured. A bridle is attached directly to the belly of the aircraft and is hooked onto the spreader bracket that protrudes from the shuttle beneath the deck.

There are many other operations that are necessary to launch a plane from a steam catapult. These other operations must follow a specific order called the launch sequence. The first thing that must occur is that the plane must be positioned above the shuttle and the bridle must also be attached to the aircraft. At the same time, steam is transported from the ship's boilers into the accumulators just below the power cylinders. The amount of steam depends on many factors that include the weight of the plane, wind conditions, and the ship's speed. Simultaneously, the exhaust valves in the power cylinders are opened to release any pressure that has built up behind the pistons.

Meanwhile the holdback and release units are attached to a cleat on the rear of the aircraft and the grab is attached to the rear of the shuttle. These two components are the trigger of the catapult. Then, hydraulic fluid is feed into the ram assembly behind the grab which will push the shuttle forward, tension the bridle and readying the plane for takeoff. Now the jet blast deflectors are raised. After a series of commands of the flight deck are given, the power cylinders are given some oil and the launching valves are opened to allow steam into the cylinder behind the pistons. When the holdback unit is released, the pistons are pushed forward through the power cylinders. This final action pulls the attached aircraft

down the runway and into the air off the deck of the carrier.

At the end of the runway on the flight deck, two more actions occur. The first action is that each of the pistons ram into a water-filled chamber known as the water brake at the end of the power cylinder. This action stops the shuttle and releases the plane. Due to the shape of the front part of the pistons, the water pressure inside the water brakes increases very quickly that will stop the piston in less than six feet. Meanwhile, another crucial action occurs. The bridle arrestor at the front of the carrier snags the bridle breaking its links to the aircraft. These links are designed to hold under the pressure of a launch and to snap away at the jot given by the bridle arrestor. After these two actions happen, the catapult can be reset to launch another aircraft (Steam 31-47).

Figure 2: Steam Catapult Force Profile (Doyle, 532)

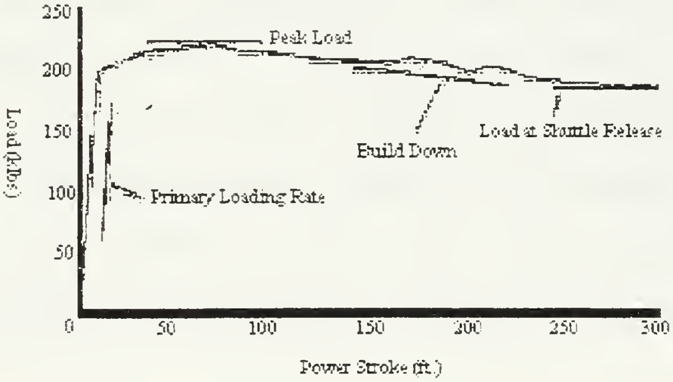

The steam catapult has had many years of operation in the fleet and has performed its assigned tasks; however, there are many inherent drawbacks in the steam system. The most important deficiency is its lack of feedback control. With the absence of feedback control, the steam system incurs large transients in the tow force of the shuttle that can damage or reduce the life of the airframe. Because of the lack of feedback and the unpredictability of the system, extra energy is added to the system to insure the minimum launch energy. This also tends to increase the unnecessary overstress on the airframe. If a closed loop control system was added to the current steam system, this control system would be very complex to significantly reduce the level of the thrust transients.

In addition to the lack of feedback control, there are many other drawbacks to the steam catapult. The steam system has a volume of 1133 cubic meters and a weight of 486 metric tons. Most of the steam catapult's weight is topside weight that can adversely affect the stability of the ship. The steam catapults are very maintenance intense and inefficient (4-6%). Also, the present operational energy limit of the steam catapult is approximately 95 megajoules. The operational energy limit needed for future payloads could increase by 30% that would push the steam system to become more complex, larger and heavier (Doyle, 528).

Figure 3: Diagram of the Steam Catapult (Navy)

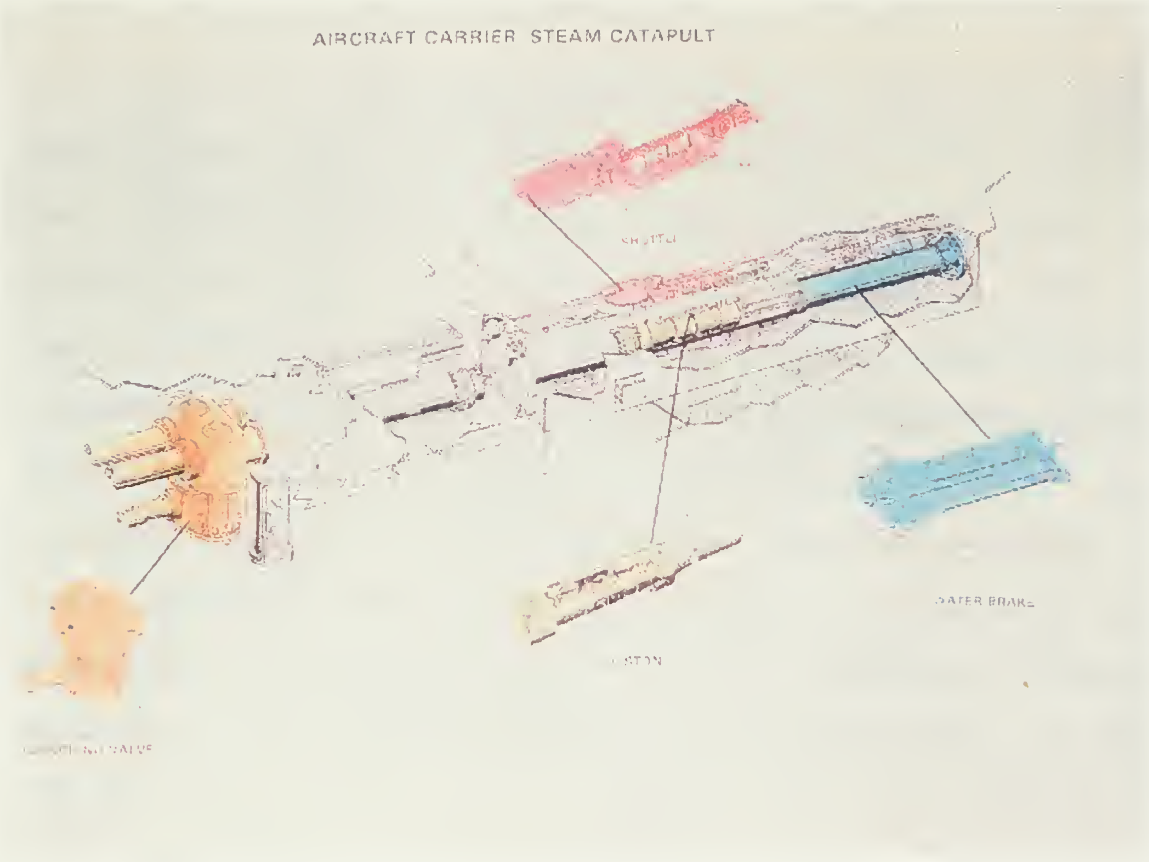

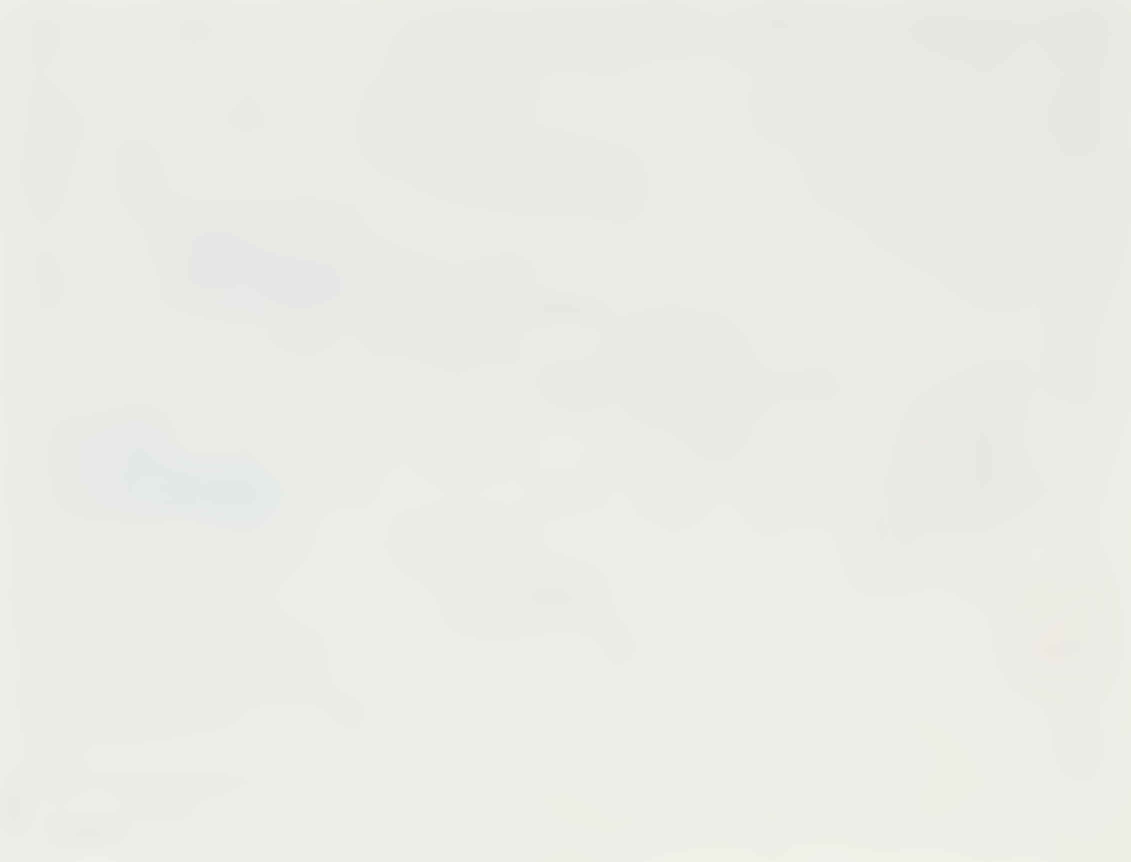

Chapter 6: The Electropult

One of the earliest linear induction motor applications was as an energy machine to launch aircraft from aircraft carriers (Boldea, 41). In the usual way, an aircraft can have the entire runway it needs in order to reach take-off speed. However, under some special circumstances the length of the runway is severely limited particularly in the case of launching aircraft from aircraft carriers. In these cases, assisted take-off is used to give the aircraft a thrust to augment the propulsion of the jet engine or the propeller. As an application for linear motors, the required speed is high enough, but also the thrust needed is very high usually in the neighborhood of 50 kiloNewtons (kN). To obtain a thrust of 50 kN with a speed of 60 meters per second (m/s) means that a power output of 3 megawatts (MW) is needed. At this power level, the only viable solution is to use what is referred to as a short stator machine. A short rotor machine would require hundreds of meters of energized track that at the time would involve the output of a moderately sized power station (Laithwaite, 153). A short stator machine is a linear machine is which the moving part is the stator that is not as long than its corresponding rotor. An illustration of this concept is shown below (Laithwaite, 59-61).

Figure 4: Short stator (a) and short rotor (b) linear machines.

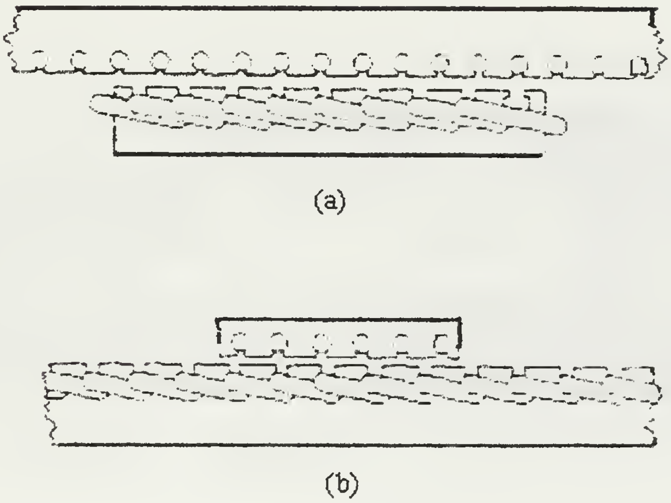

Towards the end of the last war, the Westinghouse Company of America constructed an aircraft launcher of the short stator variety. The prototype tested in 1946 was called the Electropult.

In the Electropult, the stator winding has now become the moving member. There was a penalty to be paid for the moving of the stator. Three collector brushes sliding along the slip tracks were used to supply the power input to the moving carriage. The use of these collectors led to considerable problems with the current collection in a system of this size. The current per phase was approximately 7,000 amps. The synchronous speed of the field was 100 m/s. Unfortunately, this was not the only problem with the Electropult.

Figure 5: Schematic of the Electropult

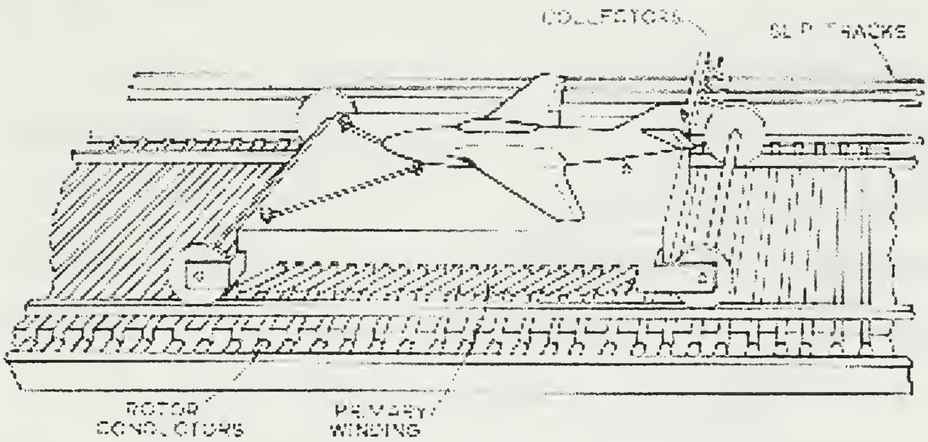

Figure (5) above shows that the layout was that of a single-sided motor where the magnetic circuit was closed by the rotor iron carrying the rotor bars in slots. It was assumed that the slot width was equal to the tooth width and also that half of the flux per pole was carried in the core. Using these assumptions with a supply frequency of 60 Hertz (Hz), the pole pitch needed is 0.82 meter with a rotor core depth of 20 cm. In addition to this, the rotor slot depth and the runway must consist of the slab or iron of around 1 meter wide and 0.3 meter thick and must contain slots to hold insulated windings. The last section of the runway was used in conjunction with D.C. braking that used 10,000 amps in order to bring the carriage to rest while the aircraft went on its way (Laithwaite, 153-154).

In 1946, two Westinghouse Electropult runways were built with one being one kilometer (km) long and the other

being 1.5 km long. The motor developed 10,000 horsepower and attained speeds over 225 mph. A 10,000-lbs. jet aircraft was accelerated from rest to 117 mph in a 540-ft run in 4.2 seconds (Boldea, 41). When the two Electropults were tested, many problems occurred. One of the problems already mentioned was the sliding collector brushes. Another serious problem that occurred was that the magnetic pull for a 50 kN driving thrust must have been accompanied by up to 500 kN of downward force. This downward force effectively multiplied the weight of the aircraft by a factor of 10.

Perhaps the most unattractive feature of the Electropult that arose during testing was that the motor was not being run at a reasonable value of slip consistent with the running economy. The carriage and aircraft never reached synchronous speed during the launch. If synchronous speed had been reached, the energy consumed in heating up the runway would have been equal to the total kinetic energy obtained. Since the synchronous speed was never reached, the heat energy exceeded the kinetic energy. Actually, the take-off speed was only 66% of the field speed. Therefore, the overall energy efficiency of the Electropult was less than 50%.

Eventually, the Electropult project was abandoned because of the high initial costs and the development of the more efficient steam catapult. A picture of the Electropult prototype follows (Laithwaite, 154-155).

Figure 6: Photograph of the Electropult Prototype

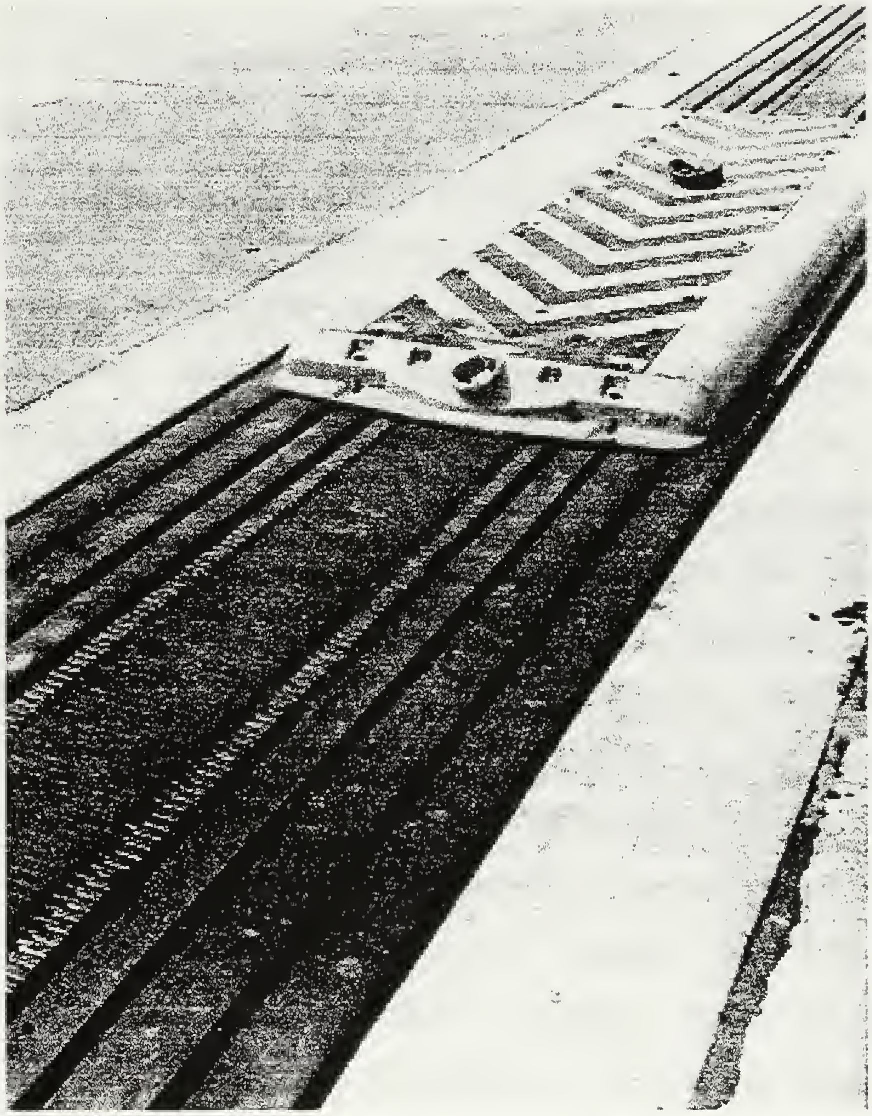

Chapter 7: The 1970's Electromagnetic Launcher Design

The investigation of new technologies for launching aircraft from ships at sea has been a continuous effort since the aircraft was first invented. The reason for this ongoing search is that the present systems offer more disadvantages than advantages.

In 1981, the Naval Air Engineering Center (NAEC) reopened investigations for the development of an aircraft catapult based on the concept of the electromagnetic launcher (Weldon, 1). This investigation was undertaken for several reasons. One of these reasons was the development of linear electric motors for use as operational high-speed ground transportation in the 1970's (Weldon, 2). Perhaps the most important reason for the investigation into the electromagnetic catapult is that the current steam catapults are a burden on the ship's resources in terms of weights, volume, and inefficiency. The linear electric motor promises a high efficiency with a low weight and volume.

In response to NAEC's search for a new aircraft launch system, Electromagnetic Launch Research, Inc. (EMLR) submitted a proposal for a new approach for the use of a linear synchronous motor to launch aircraft from a carrier. The major advantages of this approach were the use of an independent power supply and the lack of saturable iron to

limit performance. Based on these promising ideas, the NAEC began to pursue this approach (Weldon, 1).

In 1985 when the NAEC actually issued a solicitation for the development of a scale electromagnetic launcher based of EMLR's proposal, the designs were already outdated. This primary reason for this design being antiquated was the use of sliding contacts for the transmission of high levels of current to the moving armature. On the other hand, developments in the early 1980's at the Center of Electromechanics at The University of Texas at Austin (CEM-UT) produced an improved approach for an electromagnetically aircraft-launching catapult. This novel approach is a linear electric asynchronous motor that did not need either sliding contacts or sensor/switch assemblies for control. This proposal offers the most feasible design of an electromagnetic aircraft launcher to date (Weldon, 1-2).

The Electromagnetic Catapult (EMC) designed by CEM-UT is a passive, iron-free, coaxial launcher. There is no electrical contact with the armature during the entire cycle of operation. Induced currents that interact with the advancing magnetic wave excite the armature, which is the traveling shuttle. The stationary stator excited from the 60-Hertz alternating current line produces this traveling magnetic wave. It is this interaction that produces the Lorenz force that accelerates the shuttle. Essentially, the shuttle would ride the magnetic waves by

the increasing pitch, three-phase stator coils (Weldon, 5). This concept is shown in Figure (7) below (Driga, 1456).

Figure 7: Three Phase Coaxial Accelerator

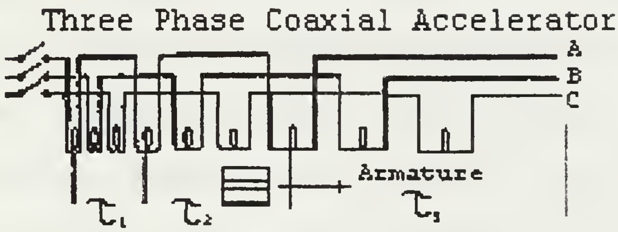

The differential velocity, or the slip, between the armature and traveling stator wave induces an armature current that can produce the necessary propelling force. The slip between the armature and field wave can be kept at low values if the time distribution of the traveling field is configured to an accelerating magnetic field. This is accomplished by increasing the pole pitch between adjacent windings like those in Figure (8) (Weldon, 6-7).

To test the viability of the proposed catapult, CEM-UT built a scaled-down version of the electromagnetic launcher that measured 12 feet. This 12-foot launcher was designed to achieve a continuous 5-g acceleration of an 18,000-lb. load. Attached to the end of the stator is a 3-foot section that is used for counter-current braking of the shuttle. This braking section is designed to stop the shuttle in the shortest possible distance. The braking is achieved by simply reversing the connector on two stator phases to the power line. This causes the traveling

magnetic wave to reverse direction. Shuttle return is accomplished by operating the electromagnetic catapult accelerator and braking coils in reverse at reduced power (Weldon, 7). Figure (8) shows a schematic of the electromagnetic launcher power system (Weldon, 8).

The three discrete stator-coil spacings were built to yield synchronous speeds of 6.6, 13.2, and 20.2 m/s. The stator coil modules are constructed separately for easy replacement. They were built using epoxy-mica paper based insulation. Passages for forced-air cooling were provided to keep the stator coil temperature below the operating limits of the insulation. The coil modules will slide into the dovetail slots in the stator-support structure as seen in Figure (9).

The electromagnetic catapult shuttle is an I-beam section of 6061-T6 aluminum with 6-mm brass plates on both sides of the central web. See Figure (10) for a diagram of the shuttle (Weldon, 11). The shuttle should be magnetically centered between the stator coils; however, a guidance system of high-speed rollers and tracks is used to ensure that the armature does not damage the stator coils.

By using two materials of substantially different conductivity in the armature, the maximum driving force under all operating conditions will minimized the reactive power. While the shuttle is accelerating, the frequency of the induced current is low (around 2.76 Hz). Therefore, the current will penetrate into the highly conductive

aluminum yielding a high efficiency and low dissipation. During braking, the frequency of the induced current will rise to approximately 120 Hz. This will result in a lesser depth of penetration that will have the armature current flow in the resistive brass aiding the braking process. The 6-mm wide vertical slots in the shuttle are used to control the eddy current pattern in the armature. A three-phase circuit breaker is used to connect and disconnect the stator windings to the 15 kV power line (Weldon, 9).

The average power per acceleration cycle for the 12-foot electromagnetic catapult is 12.62 MW. The power factor for this system is low so the apparent power required is 21.04 MVA. The energy delivered to the 18,000-lb deadload for a 5-g average acceleration to a velocity of 18.9 m/s (42.3 mph) is 1.46 MJ. The total energy delivered to the accelerator during the launch is 4.87 MJ. The gives a cycle efficiency of approximately 30% (Weldon, 11).

It should be noted that the electrical substation at the CEM-UT laboratory was used to power the launcher. Of course to meet the needs of the electromagnetic catapult, the power source must be a self-contained unit the draws the power from the ship's power plant and supplies it to the launcher.

Figure 8: Schematic of the EMC electric power system

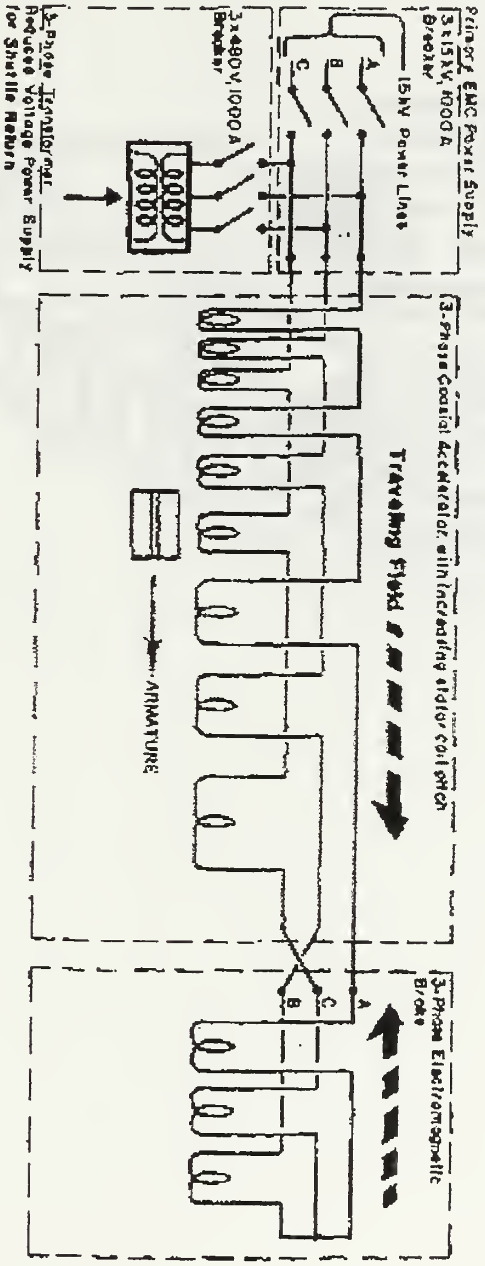
Primary EMC Power Supply
3x15kV, 1000A Breaker
15kV Power Lines
A
B
C
3x480V, 1000A Breaker
3-Phase Transformer
Reduced Voltage Power Supply for Shuttle Return
3-Phase Coaxial Accelerator with increasing stator coil pitch
Traveling Field
ARMATURE
3-Phase Electromagnetic Brake
A
C
B

Figure 9: Artist's conception of the EMC

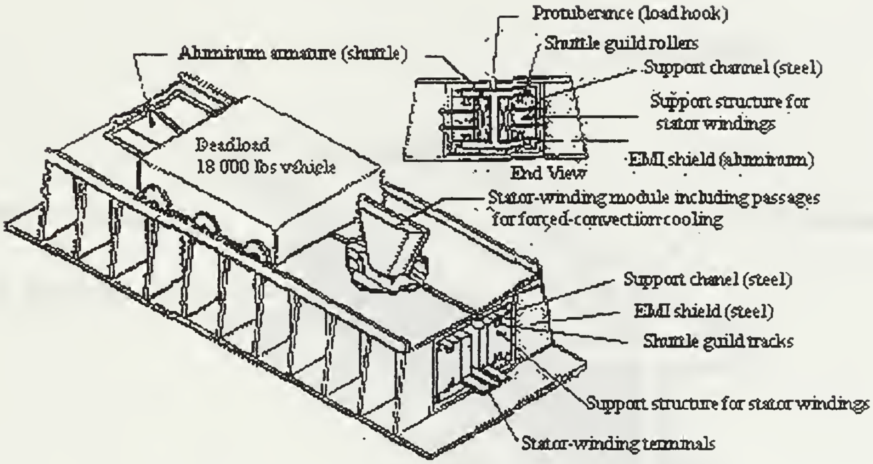
Protuberance (load hook)
Shuttle guild rollers
Aluminum armature (shuttle)
Support channel (steel)
Support structure for stator windings
Deadload 18 000 lbs vehicle
EMI shield (aluminum)
End View
Stator-winding module including passages for forced-convection cooling
Support chanel (steel)
EMI shield (steel)
Shuttle guild tracks
Support structure for stator windings
Stator-winding terminals

Figure 10: Enlarged view of the catapult shuttle

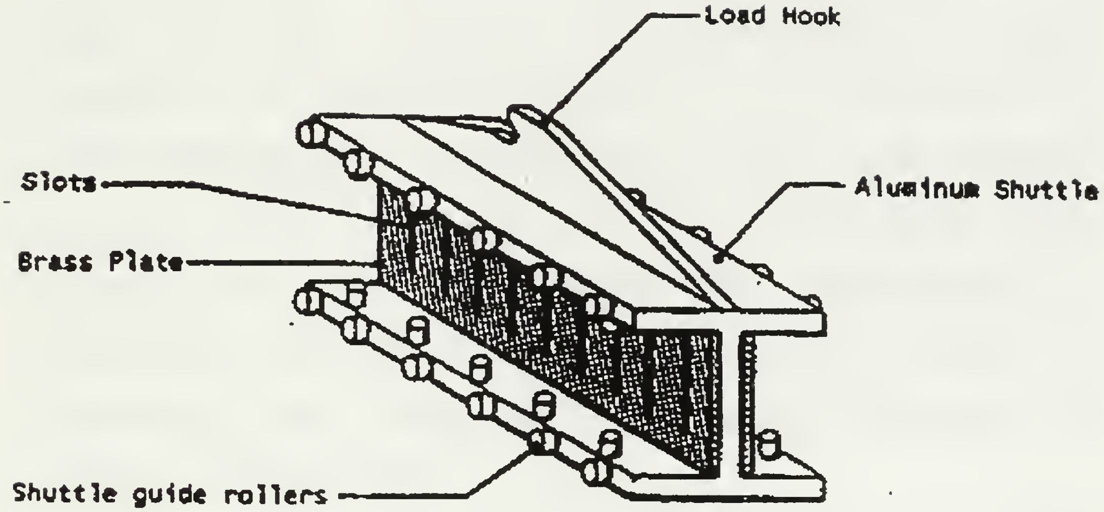

Chapter 8: Kaman's Electromagnetic Aircraft Launcher

With the new technologies in power electronics, there is new interest in electromagnetic launch systems. Of immediate concern is the application of electromagnetically catapulting aircraft from the deck of an aircraft carrier. To investigate this possibility, the U.S. Navy has commissioned a partnership between the Naval Air Warfare Center in Lakehurst, New Jersey and Kaman Electromagnetics of Hudson, Massachusetts.

The electromagnetic aircraft launcher (EMAL) that was designed by the joint Kaman-Navy venture centers on a linear synchronous motor. This motor is supplied power by four pulsed disk alternators through a cycloconverter. Using average power from an independent source on the carrier, power is stored kinetically in the rotors of the four disk alternators. Then, the alternators in a two to three second pulse during the launch release the power. This high frequency power is sent to the cycloconverter. The cycloconverter acts as an

increasing voltage and rising frequency source for the launch motor. The power is then fed into the linear synchronous motor. The linear synchronous motor accelerates the aircraft while also providing real time closed loop control. This concludes the basic launch cycle.

The beginning of the launch cycle occurs when the power from the host platform is rectified and fed into inverters. The power is then sent to the four disk alternators where it is used to spin up the rotors in the 45-second interval between aircraft launches. A diagram of the disk alternator follows (Doyle, 528-529).

Figure 11: Diagram of a Disk Alternator

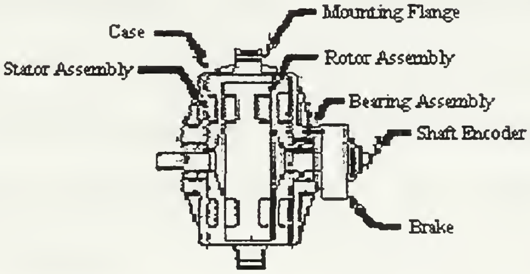

The disk alternators are permanent magnet machines with a dual stator and axial field. The

rotor serves as a kinetic energy storage component. Also, the rotor acts as a field source during power generation and is located between the two stators.

The stators each have two separate windings: one for power generation and the other for motoring. The generator windings are closer to the air gap so the reactance is reduced during pulse generation. The motor windings are put deeper in the slots which allows for better thermal conduction to the outside casing. By using high strength permanent magnets with a high pole pair number of 20, the overall active area can be better utilized. The four disk alternators are mounted in a torque frame and are paired in counter-rotating pairs that will reduce the torque and gyroscopic effects.

The disk alternator is a six-phase machine. The rotor operates at a maximum of 6400 rpm and stores a total of 121 MJ yielding an energy density of 18.1 KJ/kg. At the maximum speed, the disk alternator would give an output of 81.6 MW into a matched load. This output is at a frequency of 2133 Hz at the beginning of the pulse and 1735 Hz at the end of the pulse. The machine excitation comes from the

Neodymium-Iron-Boron 35 permanent magnets that are housed in the rotor. These magnets produced a residual induction of 1.05 Tesla and create an average working air gap flux density of 0.976 Tesla.

The stator is a radially slotted laminated core with 240 slots. This will develop a maximum back EMF of 1122 Volts. The maximum output voltage is 1700 Volts (L-L) peak. The maximum current is 6400 Amps peak per phase.

The overall efficiency of each disk alternator is 89.3% with the total losses of 127 kilowatts. These heat losses are transferred out of the disk alternator through a cold plate on the outside of the stators (Doyle, 529).

One of the reasons that the Electropult failed at the end of World War II was the lack of power electronics. It is with the new technologies in power electronics that make the EMAL a possibility. In a 103-meter long linear motor, the use of power electronics allows for an effective operation by turning only the coils that can affect the launch at a particular time rather than the entire motor at once.

The power electronics also allow for variable voltage and frequency supply.

The power electronics used in the EMAL is the cycloconverter. The cycloconverter is a naturally commutated 3ϕ-1ϕ bridge circuit. The output on one bridge is then either put in parallel or in series with the outputs of other bridges that will attain the needed power level. The output of a cycloconverter can vary from 0-644 Hertz and from 0-1520 Volts(L-L). The cycloconverter must be cooled with liquid cooling plates to dissipate the 528 kilowatts that it losses (Doyle 529).

After the power has gone from the disk alternators and through the cycloconverter, it can then be passed to the launch motor. The launch motor is actually a linear synchronous coilgun. The launch motor uses the same trough at the current steam catapults to allow for backfitting. A picture of the launch motor is shown.

Figure 12: Diagram of the Launch Motor

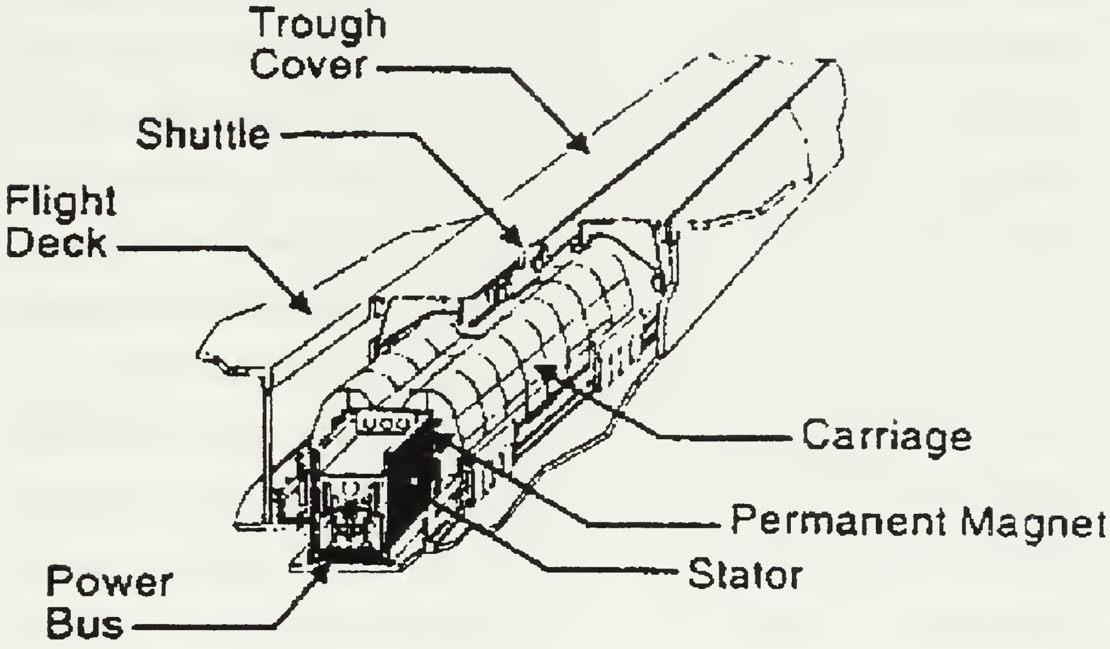

The launch motor has a dual vertical stator configuration with the active area facing outwards. The rotor of the launch motor, or the carriage, sits over the stators like a saddle and protruded through the deck so it can be attained to the aircraft. There are 160 permanent magnets of the same variety as in the disk alternator. The carriage is held in place by rollers that are welded to the stator frame. These rollers help maintain a consistent air gap of 6.35 millimeters. The stator is broken down into segments

[illegible]

that turn on and off as the carriage passes. The design also allows for the stator to be protected from the slot in the flight deck to prevent contaminants like jet fuel and hydraulic oil from possibly eroding the stator. There are busbars and static switches located in between the stators that will control the power to the stator segments.

The stator of the launch motor is divided into a modular unit called segments. The dimensions of a segment are 0.640-m long, 0.686-m high and 0.076-m wide. There are 149 segments on each side of the stator totaling 298 segments. The segment is wound as a three-phase lap winding with 24 slots and 6 turns per slot. This results into 8 poles per segment and a pole pitch of 8 cm. These coils are epoxied on a slotless stator structure which keeps the phase inductance to a low 18 μH with a phase resistance is 41 mΩ. The bus resistance is 0.67 mΩ. The flux in the air gap is 0.896 Tesla and the permanent magnets experience a shear stress of 38 psi.

After the carriage passes through the 103-meter power stroke, the front of the carriage will enter the brake. The brake is made up of shorter stator

segments which bring eddy current brakes. At the same point in time, the carriage is still covering a number of active stator segments. Two of the phases are switched in these end segments so that a reverse thrust is initiated to create a braking force.

The launch motor has a projected efficiency of 70% and has peak losses of 13.3 MW. With this lack of efficiency, active cooling will be necessary. The launch motor uses an aluminum cold plate to remove the heat from the attached stator windings and back iron. The carriage that houses the permanent magnets can be cooled by convection since they will experience only slight heating from eddy currents in the carriage structure and magnets (Doyle, 530).

Figure 13: EMAL Force Profile

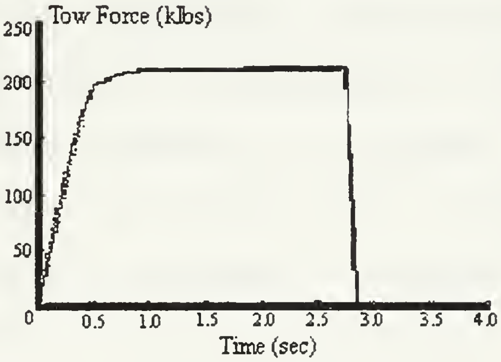

The overall design of the EMAL designed by the joint Kaman-Navy venture offers many benefits over the present steam catapult. The launch engine is capable of a high thrust density. The half-scale test model produced 1322 psi while the current steam catapult produces only 450 psi. Also, the new launch motor will require much less manpower to operate and maintain. The EMAL has been designed to by self-diagnostic rather than the substantial manual inspection required on the steam catapult. Another advantage of the EMAL is that it is a stand-alone system. The present steam system requires many subsystems including hydraulics, water braking and control systems.

Unfortunately, the EMAL proposed by Kaman Electromagnetics has a few drawbacks. One of the drawbacks is that high power electromagnetic motors create electromagnetic interference with electronic equipment. This presents a problem because the aircraft that will be launch has a large amount of sensitive electronic equipment. Another drawback of this EMAL design is the disk alternators. These high-speed pieces of rotating machinery are spinning at

about 6400 rpm storing a total of 484 MJ. While these disk alternators work in a laboratory setting, the jarring and motion of an aircraft carrier could cause the disk alternators to be less effective and possibly even malfunction (Doyle, 531).

The electromagnetic aircraft launcher design by Kaman Electromagnetics is a step in the right direction for replacing the current steam catapult. The EMAL offers many advantages but does have a few drawbacks.

SECTION III: THEORY OF LINEAR INDUCTION LAUNCHER

Section III consists of a review of the theory of the electromagnetic launchers. Chapter 9 is a discussion of the two different types of electromagnetic launchers: the railgun and the coilgun. Chapter 10 is a review of the stress that can exist in electromagnetic launchers. An idealized model of a coilgun is presented in Chapter 11. Chapter 12 discusses the limitations of the coilgun. Chapter 13 describes the various scaling factors for the models of linear induction launchers. Finally, Chapter 14 is a study of what occurs at the transition between two sections of a linear induction launcher.

Chapter 9: The Railgun and the Coilgun

For the design of the electromagnetic catapult, a review of various tubular motors must be discussed. In particular, two types of tubular motors that merit an in-depth examination are the railgun and the coilgun.

In all linear induction machines, the total energy stored in a LIM is proportion to the product of the mutual inductance between the primary and secondary, the primary current and secondary. Equation (1) follows:

$$W = \frac{1}{2}\sum_{i=1}^{N}\sum_{j=1}^{N} L_{ij} I_i I_j \qquad (1)$$

L_{ij} is the mutual inductance of the two coils. I_i and I_j are the two currents and N is the number of coils. The coenergy of a linear system (W_c) is the product of the currents and the flux linkages minus the energy. In linear systems, the energy and coenergy are equal. The force exerted by a linear system is the first-order derivative of the coenergy

with respect to the unit length of the system. Equation (2) follows:

$$F = \frac{dW_c}{dz} \qquad (2)$$

Therefore, the total force exerted on the projectile of a linear system follows as Equation (3) where z is the direction of displacement (Mongeau, 227).

$$F = \frac{1}{2}\sum_{i=1}^{N}\sum_{j=1}^{N}\frac{dL_{ij}}{dz}\,I_i I_j \qquad (3)$$

Figure 14: The basic diagram of a railgun. (Calvin, 107)

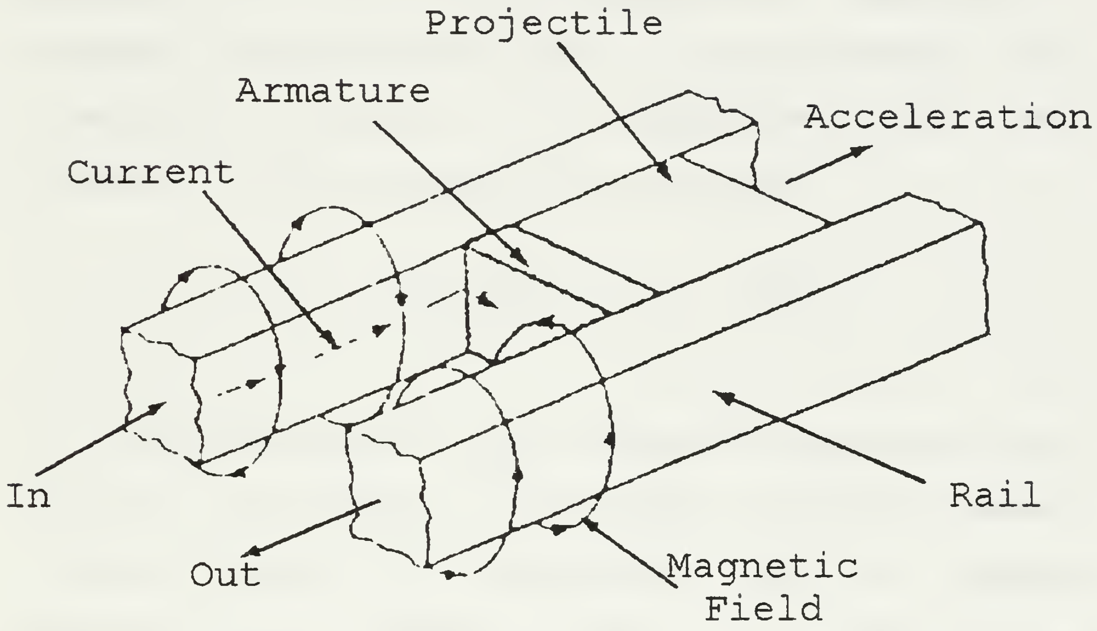

Now that the general equations governing a linear system have been established, the above principles can be applied to a specific system commonly referred to as the railgun. Railguns are a simple homopolar structure. They make use of the Lorenz force to accelerate projectiles to very high velocities. The acceleration force is developed in the sliding contact connecting the rails. In the case of the railgun, the armature pushing the projectile is used to complete the circuit with the rails. Thus producing the

[illegible]

magnetic field. The railgun follows the same general equation for linear induction machines (Equation 3). Because the railgun has only a single winging (i.e. homopolar), equation (3) simplifies with N=1. Equation (4) for railguns is as follows:

$$F = \frac{1}{2} L'I^2 \qquad (4)$$

The inductance of the railgun is given per unit length. This equation is for ideal situations where a constant current is maintained. For the typical values of an armature current of 1 MA and an inductance of 0.4 μH/m, the resulting force is 200 kJ per meter of gun.

Some of the basic principles of the railgun merit discussion. Because the rails must be very conductive, the overall impedance of the rails is very low. This results in a very high current, which can be seen in the previous example. Another basic principle of the railgun is the high velocity of the projectile.

The railgun also contains many disadvantages that merit discussion. One of the most important parts of

the railgun is the connection of the rails and the projectile by sliding contacts. These sliding contacts produce friction and cause a significant loss in efficiency. Also, the design of the railgun given only two adjustable parameters: the self-inductance of the rails and the current. Unfortunately, the inductance is difficult to increase without the use of augmented rails that acts as multiple rails. This leaves only the current as an adjustable parameter. In order to maintain any constant current, multiple energy storage devices must be used. Another disadvantage is that the flux in the rails will produce a normal force on the projectile. This normal force can be in either direction perpendicular to the rails depending on the direction of the current (Mongeau 227-299).

Another type of tubular motor that requires attention is commonly referred to as the coilgun. The basic design of the coilgun is similar to that of a conventional rifle. In this case, the barrel of the conventional gun is similar to the primary winding of the coilgun. The bullet of the conventional gun becomes the projectile (or secondary winding) of the

coilgun. In a two winding system, Equation (2) simplifies with N = 2 into Equation (5):

$$F = \frac{1}{2} I_1^2 \frac{dL_{11}}{dz} + \frac{1}{2} I_1 I_2 \frac{dL_{12}}{dz} + \frac{1}{2} I_2 I_1 \frac{dL_{21}}{dz} + \frac{1}{2} I_2^2 \frac{dL_{22}}{dz} \qquad (5)$$

The force that each coil’s inductance does to itself is independent of z. Also, L_{12} and L_{21} are equal to the mutual inductance (M) between the primary and secondary windings.

Therefore, Equation (5) simplifies

$$F = \frac{dM}{dz} I_p I_s \qquad (6)$$

where I_p and I_s and the currents in the primary and secondary windings.

The mutual inductance between the two coils needs explanation. In two filamentary loop of radius a and b, the mutual inductance can be defined as

Equation (7):

$$M = \mu k\sqrt{ab}\left[\left(\frac{2}{k} - k\right)K(k) - \frac{2}{k}E(k)\right] \qquad (7)$$

$$\textit{where} \qquad k^2 = \frac{4ab}{z^2 + (a+b)^2}$$

Where E(k) and K(k) are elliptic integrals of the first and second order respectively. This equation for mutual inductance behaves similarly to a decaying exponential with relation to the z-axis. Also, the mutual inductance is symmetric about the z-axis. An example is for coils with radii of 6 cm and 5 cm, the mutual inductance drops to less than six percent of its peak at a distance of 10 cm, which is the diameter of the secondary coil.

Figure 15: The basic geometry of a coilgun (McKinney, 239).

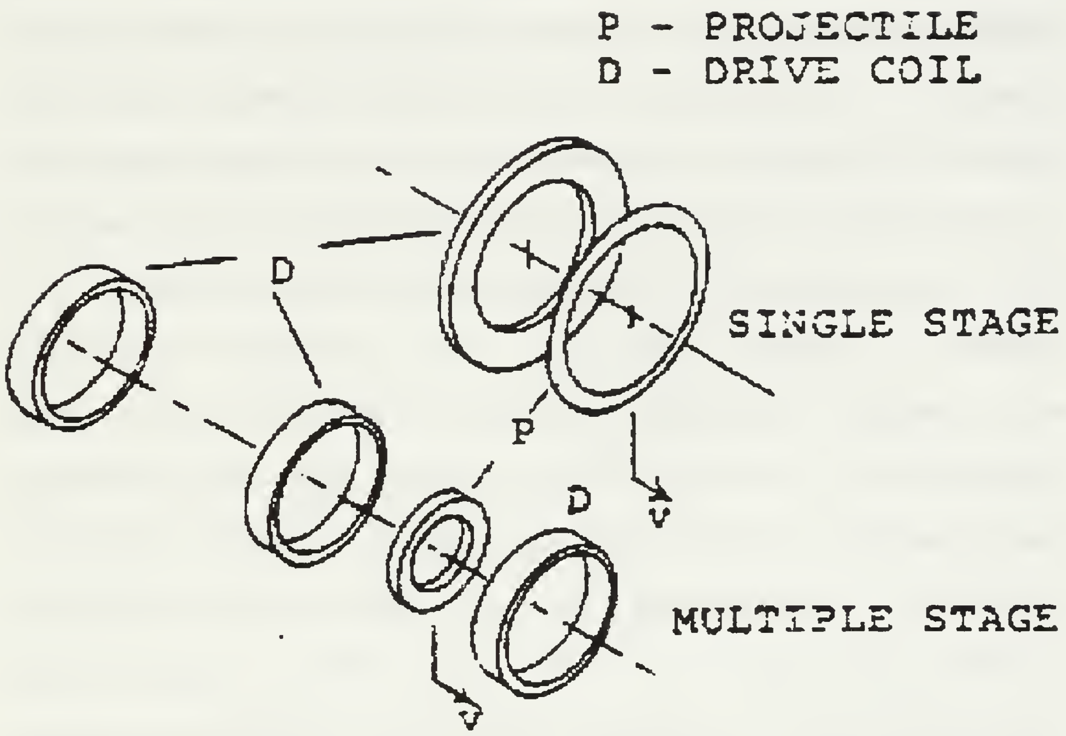

Some basic principles of the coilgun need explanation. Because of the symmetric design of the coils, the coils will attract each other if the coils are polarized in the same direction. This will cause the radial force to be positive. Also, the mutual inductance tends to be higher than that of a railgun. This results in relatively high impedance. Also, the force of the coilgun is dependent on two currents: the primary current and secondary current. This means

[illegible]

[illegible]

[illegible]

[illegible]

that the two currents in the coils need not be nearly as high as the current needed in a railgun. Also, the coilgun does not have the need of the contact brushes. This will greatly improve the efficiency. It should be noted that the coilgun needs the constant currents in the coils to provide stability and help efficiency.

One of the best advantages of the coilgun is the inherent flexibility in its basic design. Because more than one coil will be generally needed, the dimensions of the primary coils need not be constant. This will provide changes in the mutual inductance and therefore the force on the projectile. This is particularly useful when the final velocity must be reached gradually to prevent damage to the projectile. This can also be used for a braking action to gradually slow down the projectile (McKinney, 239-242).

Coaxial launchers received sporadic attention in previous research while the focus of development has on the railgun. The primary reason for this emphasis has been for the same reason that early aeronautical research was directed towards dirigibles: they are simpler. Coaxial launchers (i.e. coilguns) are like

airplanes having certain unique advantages that are impossible but at a price of a much higher complexity. One of these advantages is that no physical contact through brushes is required in the coaxial launcher but is necessary in the railgun. As a result of a lack of physical contacts, coaxial launchers have potentially no wear. Coaxial launchers are more easily scaled up to very large projectile sizes (Kolm, 227). The thrust in a coaxial launcher acts over the entire length of the projectile that consequently reduces the mechanical stresses (Levi, 1). For a given current, the coilgun will produce up to 100 times more thrust than a railgun. Also, coaxial launchers can achieve efficiencies over 50 percent (Kolm, 227). In railguns, the energy acquired by the projectile cannot exceed the energy left behind in magnetic form which means that the efficiencies cannot exceed 50 percent (Levi, 1). Another characteristic of the coaxial launcher that is advantageous is that there is positive control during the entire launch cycle. Also, megampere input connections are not necessarily required by coilguns. Finally, the coaxial launcher

is built of individually replaceable, self-supporting coils.

The price for all of these advantages is the need for a drive current in the form of precisely synchronized pulses with transit of each projectile coil through each drive coil. This can be easily accomplished by commutation of an oscillatory system at zero-crossings, but at high velocities this required high voltages. Therefore, the coaxial launcher technology can be limited by high voltage switching technology (Kolm, 227).

In general, railguns are of a much simpler design than coaxial launchers. Also, railguns are much easier to manage than coilgun particularly in the area of energization. This simplicity in railguns does have drawbacks. The efficiency of railguns is limited while coilguns can achieve very high efficiencies. Also, coilguns unlike railguns require no physical contact which significantly reduces friction and erosion. Railguns require much higher currents levels (up to 10 times higher) for a given thrust than a coaxial launcher does. Most importantly, the coaxial launchers represents a much more flexible machine with

higher efficiency and lower current levels but with higher levels of complexity than the railgun.

Chapter 10: Stresses on Electromagnetic Launchers

Ideally, an electromagnetic launcher should be designed to achieve a given muzzle velocity using the shortest barrel length possible. This means that the acceleration should be as high as possible while maintaining consistency with the strength of the material. The armature of the projectile is subjected to mechanical, electromagnetic, and thermal stresses, which are impulsive in character. Therefore, in order to separate their effects, it is useful to determine the order of magnitude of the speed with which each stress propagates.

Mechanical stresses propagate with the velocity of sound that is in the order of (10^3) m/s in solids. Since the materials of interest are good conductors, the propagation of the electromagnetic and thermal stresses is governed by diffusion equations. Introducing a characteristic length (L) and α is the diffusivity, the diffusion velocity can be defined (v_d) as equation (8).

$$v_b = \frac{\alpha}{L} \qquad (8)$$

By defining electrical conductivity (γ) and the magnetic permeability (μ), the diffusivity of the electromagnetic stress ($\alpha_{e,m}$) can also be defined as equation (9).

$$\alpha_{e,m} = \frac{1}{\gamma\mu} = O(10^{-1}) \qquad m^2 / s \qquad (9)$$

With a characteristic length of 1 cm (L=0.01 m), this equation will correspond to a velocity of 10 m/s. By denoting the heat conductivity (λ) and the specific heat per unit volume(c), the thermal diffusivity be obtained

$$\alpha_t = \frac{\lambda}{c} = O(10^{-4}) \qquad m^2 / s \qquad (10)$$

This thermal diffusivity corresponds to a velocity of 10^{-2} m/s.

These large differences in the propagation velocities of the mechanical, electromagnetic, and thermal stresses suggest the following assumptions. The mechanical stresses are established instantaneously. Next the electrical stresses are

established. Finally, all of the heat is dissipated in one skin depth and is absorbed locally in a thermal process that is adiabatic.

These assumptions allow some general relationships to be derived for a unit volume of the projectile armature. $\underline{J}$ denotes the current density. $\underline{B}$ represents the magnetic flux density. The mass density of the armature conductor is denoted ξ. The ratio of the overall mass of the projectile to the mass of the armature conductor is represented by ν. The temperature rise over the ambient temperature is denoted by θ. Neglecting friction losses, the increment of kinetic energy from the breech velocity (v_b) to the muzzle velocity (v_m) equates to the work done by the electromagnetic force ($\underline{J} \times \underline{B}$) over the length of the barrel (l) represented.

$$\Delta w_{kin} = \frac{1}{2} \nu \xi \left(v_m^2 - v_b^2 \right) = \int_0^l \underline{J} \times \underline{B} \cdot d\underline{l} \qquad J / m^3 \qquad (11)$$

The energy dissipated in the conductor is shown in equation (12).

$$w_{diss} = \frac{J^2}{\gamma} \cdot \frac{l}{\left(v_m + v_b \right) / 2} = c\theta \qquad J / m^3 \qquad (12)$$

In the ideal case with a perpendicular orientation of the vector J, B, and dl and a uniform distribution, J can be eliminated to obtain equation (13).

$$\left(v_m^2 - v_b^2\right)\left(v_m - v_b\right) = \frac{2c\gamma\theta}{v^2\xi^2} B^2 l \qquad (13)$$

It can be seen that as v_b approaches zero that the length l of the barrel increase as the cube of the muzzle velocity represented in equation (14) (Levi, 1-2).

$$l = \frac{v^2\xi^2}{2\gamma\ c\ \theta\ B^2} v_m^3 \qquad (14)$$

Chapter 11: Idealized Model of a Coilgun

The model of the idealized coilgun has many components and considerations. The first of the considerations is the number of stages. The force acting on the coil that guides the projectile in the single stage coilgun has an effective range of less than one coil diameter. A single stage coilgun consists of two coils (Kolm). To obtain the higher velocities, a multistage arrangement is needed in which the barrel consists of an array of coils energized synchronously with the progression of the projectile. In addition to lower speeds, the motion of a single projectile stage might also be expected to be unstable against lateral diversion and tumbling. Therefore, more than one coil is necessary in the projectile.

Another important consideration in coilgun design is the stresses. Because of the limitations imposed by the strength of the material, the stresses need to be distributed as evenly as possible in both space and time.

An arrangement for a coilgun that satisfies these requirements is shown in Figure (16). The barrel coils are energized in a polyphase fashion to create a traveling electromagnetic wave packet of limited extent. Similarly the discrete coil in the projectile is replaced with a continuous tubular conductor in the shape of a sleeve of sufficient length to accommodate a number of wavelengths. Then the thrust results from the interaction of two systems of the azimuthal currents sinusoidally distributed in the longitudinal direction. The currents flowing in the sleeve are impressed in the first stage of the barrel and the sleeve thickness must be sufficient so that the time it takes them to decay is longer than the transit time (T) of the projectile in the barrel.

Figure 16: Polyphase barrel with sleeve projectile

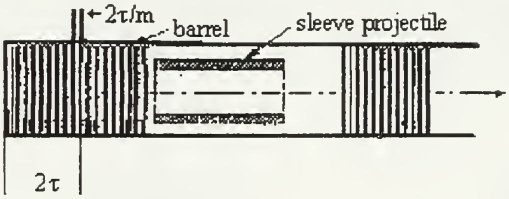

The design of the coilgun can now be based on the idealized model of conventional electrical machines. By letting the thickness of the conductor be negligible, the current distributions in the sleeve and in the barrel can be reduced to surface current sheets. Also, it is practical to neglect the curvature of the conductors to deal with planar sheets. The new model is shown below (Levi, 2-3).

Figure 17: Planar sheet model of coilgun

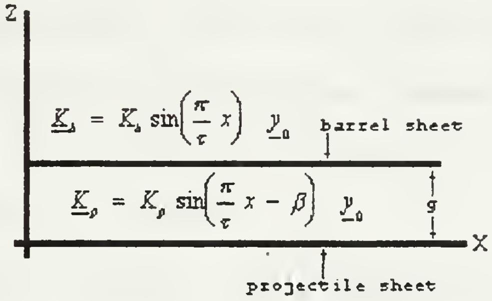
Z
$\underline{K}_b = K_b \sin\left(\frac{\pi}{\tau} x\right) \ \underline{y}_0$
barrel sheet
$\underline{K}_p = K_p \sin\left(\frac{\pi}{\tau} x - \beta\right) \ \underline{y}_0$
g
X
projectile sheet

The current distributions in the projectile ($\underline{K}_b$) and in the barrel ($\underline{K}_p$) are as follows where τ is the pole pitch.

$$\underline{K}_b = K_b \sin\left(\frac{\pi}{\tau} x\right) \quad \underline{y}_0 \tag{15}$$

$$\underline{K}_p = K_p \sin\left(\frac{\pi}{\tau} x - \beta\right) \quad \underline{y}_0 \tag{16}$$

Solving Maxwell's equations, the magnetic flux density (B_{bz}) and magnetic field intensity (H_{bx}) produced by $\underline{K}_b$ in the plane of the sleeve located at a distance (g) is defined:

$$H_{bx} = -\frac{K_b}{2}\sin\left(\frac{\pi}{\tau}x\right)e^{-\frac{\pi}{\tau}x} \qquad (17)$$

$$B_{bz} = \mu_0\frac{K_b}{2}\cos\left(\frac{\pi}{\tau}x\right)e^{-\frac{\pi}{\tau}x} \qquad (18)$$

At a distance (g), the local value of the force per unit surface acting on the sleeve is defined:

$$\begin{aligned}\underline{f}_p &= \underline{K}_p \times \underline{B}_b \\ &= \mu_0 K_p\frac{K_b}{2}e^{-\frac{\pi}{\tau}g}\sin\left(\frac{\pi}{\tau}x - \beta\right)\bullet\left[\cos\left(\frac{\pi}{\tau}x\right)\underline{x}_0 + \sin\left(\frac{\pi}{\tau}x\right)\underline{z}_0\right] \qquad (19)\end{aligned}$$

The average local value of the force per unit surface (N/m^2) can then be obtained:

$$\left\langle\underline{f}_p\right\rangle = -\mu_0 K_p\frac{K_b}{4}e^{-\frac{\pi}{\tau}g}\left[\sin(\beta\underline{x}_0) - \cos(\beta\underline{z}_0)\right] \qquad (20)$$

Given that the maximum allowable mechanical stress (σ_m) is defined as:

$$\sigma_m = K_p B = \frac{B^2}{\varepsilon\mu_0} \quad (N / m^2) \qquad (21)$$

Equating the mechanical stress (σ_m) with the average force density in Equation (20) gives the following relationship (Levi, 3):

$$K_p = \frac{4\sigma_m}{\mu_0 K_b} e^{\frac{\pi}{\tau} g} \qquad (22)$$

Let ξ represent the mass density of the armature conductor and ν be the ratio between the overall mass of the projectile to the mass of the armature conductor. By integrating Newton's law between the breech and muzzle velocities (v_m and v_b respectively), the following relations can be obtained:

$$\nu\xi(v_m - v_b) = \frac{\langle f_p \rangle_x}{a_p} T = \frac{\langle f_p \rangle_x}{a_p} \frac{2c\theta a_p^2 \gamma}{K_p^2} = \frac{\mu_0 K_b e^{-\frac{\pi}{\tau} g} \theta \quad a_p \gamma \quad c \sin\beta}{2K_p} \qquad (23)$$

The following relations where used to in Equation

$$c\theta = \frac{J^2}{\gamma}\, T = \left(\frac{K_p}{a_p}\right)^2 \frac{T}{\gamma}$$

(23).

By using the definition of K_p in Equation (22), the following definition for K_b can be found:

$$K_b^2 = \frac{8\nu\xi(v_m - v_b)\sigma_m}{\mu_0^2 c\theta\gamma \sin\beta}\, \frac{1}{a_p e^{-2\frac{\pi}{\tau}g}} \qquad (24)$$

The distance between the equivalent current sheets is a function of the thickness of the barrel and projectile conductors (a_b and a_p respectively). Let g_c be the clearance between the barrel and the sleeve, which is usually less than 1 mm. The distance can then be defined:

$$g \approx g_c + \frac{a_b + a_p}{2} \qquad (25)$$

By utilizing this value of g into Equation (23), it can be found that the minimum value of K_b is reached when $a_p = \pi/\tau$ (Levi, 3).

Now Equation (23) gives the new ratio:

$$\frac{K_b}{K_p} = \frac{\pi}{\tau}\frac{2v\xi(v_m - v_b)}{e^{-\frac{\pi}{\tau}g}c\theta\mu_0\gamma} \qquad (26)$$

By letting $a_b = a_p$ and neglecting g_c, the following ratio can be found:

$$\frac{\pi}{\tau}g \approx 1 \qquad (27)$$

Instead, solving Equation (23) for a_p yields:

$$a_p = \frac{1}{\left(\frac{e^{-\frac{\pi}{\tau}g}}{2}\frac{K_b}{K_p}\sin\beta\right)}\frac{v\xi(v_m - v_b)}{\mu_0\gamma c\theta} \qquad (28)$$

Because this sleeve thickness has been obtained on the basis of thermal considerations, it should be checked to verify that it also satisfies structural requirements (Levi, 3-4).

Using the length of the barrel as a determination, the thickness of the armature conductor (a_p) can be found in another manner. By using

Equations (11), (13), and (21), the armature conductor thickness turns out to be:

$$a_p = \sigma_m \frac{l}{\Delta w_{kin}} = \frac{v}{\varepsilon} \frac{\xi(v_m - v_b)}{\mu_0 \gamma c \theta} \qquad (29)$$

Comparing Equations (28) and (29), a value for ε can be found:

$$\varepsilon = \frac{e^{-\frac{\pi}{\tau} g}}{2} \frac{K_b}{K_p} \sin \beta \qquad (30)$$

$$K_b = K_p = \frac{B}{\varepsilon \mu_0} \qquad (31)$$

When this value is compared to the corresponding one for a railgun, the following relation is found:

In the ideal case of a railgun, the coaxial structure has ε = ½. Also with a parallel structure, it can be assumed that β = 45°. This supports the conclusion that in order to obtain the same thickness a_p in a coilgun as in a railgun that the following must be true:

$$\frac{K_b}{K_p} = \sqrt{2} \quad e^{-\frac{\pi}{\tau} g} \qquad (32)$$

By using the relation in Equation (32), the following value can be found:

$$\frac{K_b}{K} \approx 3.83 \qquad (33)$$

It would be difficult to accommodate a much larger K in the barrel while keeping $a_b = a_p$. A much larger a_b would increase the value of g and would therefore decrease the coupling between barrel coils and projectile sleeve. From these relationships, it must be concluded from Equation (28) that the thickness of the moving conductor of the coilgun must be larger than that of the railgun (Levi, 6). This fact when combined with the fact that the need for strong coupling sets a lower limit of approximately two inches for the diameter of the sleeve and because of stability considerations, it is desirable to accommodate at least one wavelength in the length of the sleeve (Kolm). All of this leads to the conclusion that coilgun projectiles must be much heavier than those in railguns must.

Chapter 12: The Limits of the Coilgun

While coilguns are conceptually simple, they are extremely difficult to design. The normal method for coilgun design is a "cut-and-try" approach in which the performance of a trial design are predicted and design parameters are adjusted until the performance goals are met. While design procedures that make use of the formal optimization techniques have been proposed, they are extremely expensive to operate and give little insight of the interdependence of design performance and parameters (Williamson, "Application," 258). The following is an exploration into the maximum velocity achievable.

The investigation will be based on a simple system of two coaxial air-cooled coils carrying the currents i_1 and i_2 respectfully. This design is shown below.

Figure 19: Filamentary coaxial coils

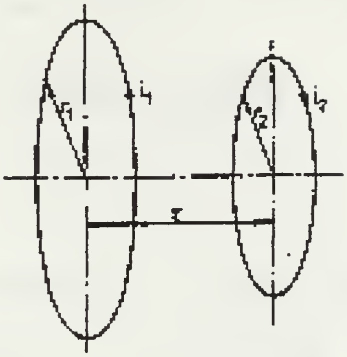

Equations (6) and (7) are the basis of the exploration.

$$F = \frac{dM}{dz} I_1 I_2 \qquad (6)$$

$$M = \mu_0 \sqrt{r_1 r_2}\left[\left(\frac{2}{k} - k\right)K(k) - \frac{2}{k}E(k)\right] where \quad k^2 = \frac{4 r_1 r_2}{z^2 + (r_1 + r_2)^2} \qquad (7)$$

Assuming that the outer coil is stationary and the inner coil is free to move, the work done when the inner coil moves from z_1 to z_2 is

$$W = \int_{z_1}^{z_2} F dz = \int_{z_1}^{z_2} i_1 i_2 \frac{dM}{dz} dz \qquad (34)$$

Now be hold the two currents constant at their maximum values, then Equation (34) becomes

$$W = i_1 i_2 \left[M(z_2) - M(z_1) \right] \qquad (35)$$

Ignoring mechanical losses and joule losses in the armature coil, the maximum kinetic energy is achieved when equation (35) is maximized. The maximum value of M(z) occurs at z = 0, and the minimum value occurs at z = ∞. This yields the following relation with M(∞) = 0 (Williamson, "Pulsed," 201).

$$KE_{\max} = i_1 i_2 M(0) \qquad (36)$$

This shows that the maximum kinetic energy is obtained if the coils are co-planar and the currents are held at the maximum values. In a real system, the currents cannot be instantaneously switched to the maximum value. In particular, the current in the inner coil will vary with time.

Figure 20: Thin pancake coils

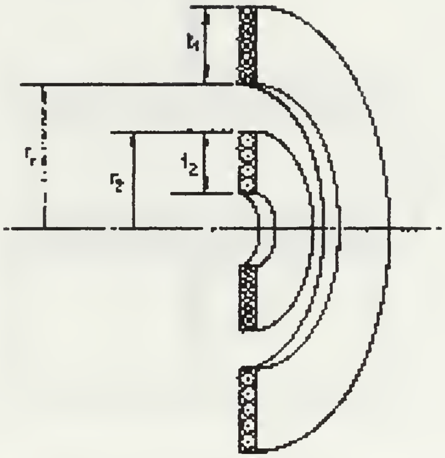

In Figure (20) above, thin pancake coils have replaced the filamentary coils. The basic form of equation (36) holds true although the mutual inductance must now be an average over the radial width of the coils. By letting the coils have N_1 and N_2 turns respectfully and neglecting the axial length, equation (36) can now be replaced with

$$KE_{\max} = i_1 i_2 N_1 N_2 \frac{1}{t_1 t_2} \int_{r_1}^{r_1 + t_1} \int_{r_2 - t_2}^{r_2} M(0) dr_1' \, dr_2' \qquad (37)$$

Figure 21: Armature coil with finite length

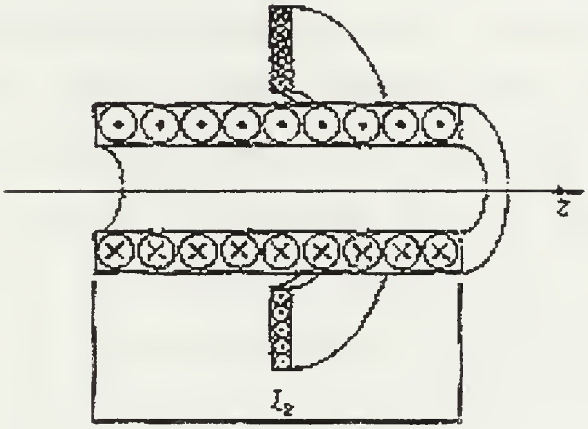

Next, it will be assumed that the armature coil has a finite length of l_2 as shown above in Figure (21). Under the maximum current assumption, it can be found that the maximum kinetic energy is obtained when the initial position of the armature coil is symmetrical to the pancake coil. This results in the following equations (Williamson, "Pulsed," 201-202).

$$KE_{\max} = i_1 i_2 N_1 N_2 \frac{1}{t_1 t_2 l_2} \int_{r_1}^{r_1+t_1} \int_{r_2-t_2}^{r_2} \int_{-\frac{l_2}{2}}^{\frac{l_2}{2}} M(r_1', r_2', z)\, dr_1'\, dr_2'\, dz \tag{38}$$

$$= \frac{i_1 i_2 N_1 N_2}{t_1 t_2 l_2} S \tag{39}$$

$$\text{where} \quad S = \int_{r_1}^{r_1+t_1} \int_{r_2-t_2}^{r_2} \int_{-\frac{l_2}{2}}^{\frac{l_2}{2}} M(r_1', r_2', z)\, dr_1'\, dr_2'\, dz \tag{40}$$

The final stage in the development of this model is to give the stator coils a finite length of l_1. In doing so, it will be assumed that all of the stator coils to the left of the armature are energized and those to the right are not energized. As the armature moves, the current is assumed to be instantaneously switched into the stator coils that lie on the centerline. It is now necessary to let N_1 to represent the total number of turns in the stator. This layout is shown below.

Figure 22: Stator coil and armature excitation

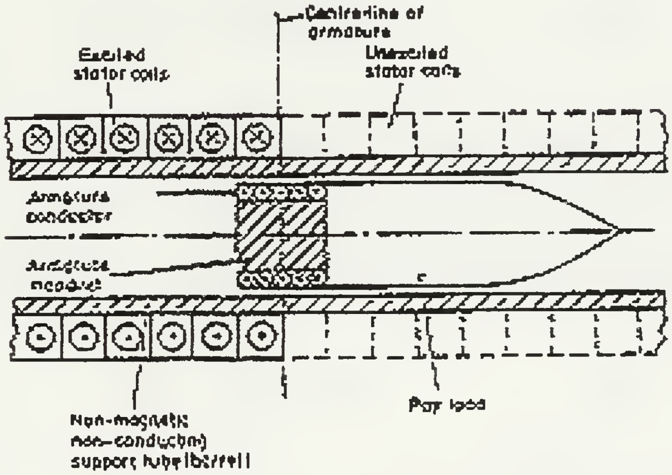

Because the current and turn numbers are often scaled to suit supply conditions, they will be removed with the following relations.

$$i_1N_1 = J_{c1}k_1t_1l_1 \qquad (41)$$

$$i_2N_2 = J_{c2}k_2t_2l_2 \qquad (42)$$

J_{c1} and J_{c2} are the current densities in the stator and rotor respectfully. k_1 and k_2 represent the ratio of the copper section to winding section of a coil. l_1 and l_2 are the axial lengths of the stator and armature. Substituting equations (41) and (42) into (39),

$$KE_{\max} = J_{c1}J_{c2}k_1k_2l_1S \qquad (43)$$

If it is assumed that an inert projectile of mass m is accelerated from rest by an armature of mass αm to a velocity v, then the kinetic energy gained is

$$KE = \frac{1}{2}(1 + \alpha)mv^2 \qquad (44)$$

Where α is the ratio of the armature mass to the projectile mass.

Combining equations (43) and (44) yields (Williamson, "Pulsed," 202-203).

$$(1+\alpha)m_{\max}^2 = 2J_{c1}J_{c2}k_1k_2l_1S \tag{45}$$

It can be assumed that the mutual inductance between the coils falls rapidly as the distance between them increases. Even in the ideal coilgun, the current in a given stator coil will be reduced to zero when the armature has passed it by a distance equivalent to two or three diameters. Furthermore, being stationary the stator coils are more readily cooled. It can therefore be assumed that the thermal limits will not be approached on the stator. On the other hand, the armature currents are required to endure for the entire time that the armature is inside the barrel and for a short distance beyond the bore. By assuming that the armature heats adiabatically, the rate of temperature rise in the armature copper is

$$\frac{d\theta}{dt} = \frac{J_{c2}^2\rho T}{C_p d} \tag{46}$$

C_p is the specific heat of the copper, ρ is its resistively, and d is its density. As the armature current is assumed to be constant, the temperature rise obtained in time T where the parameters are not temperature dependent is given as (Williamson, "Pulsed," 203)

$$\theta = \frac{J_{c2}^2 T \rho}{C_p d} \qquad (47)$$

Now that the kinetic energy and thermal limits have equations defining their effects, the importance of the mechanical stress can be found. The axial flux density at the inside surface of the stator is obtained by the long solenoid approximation as

$$B_{z1} = \mu_0 J_{c1} k_1 t_1 \qquad (48)$$

The radial stress that this will produce is

$$P_s = \frac{1}{2\mu_0} B_{z1}^2 = \frac{\mu_0}{2} \left[J_{c1} k_1 t_1 \right]^2 \qquad (49)$$

By using the standard approximation for a long solenoid that the magnetic field outside the solenoid is negligible, the radial stress is also approximately zero. The hoop stress in the stator varies across the

radial thickness of the stator with the magnitude occurring at the inner surface. The maximum of the stress is

$$\sigma_{\max} = \frac{P_s\left(r_1^2 + \left(r_1 + t_1\right)^2\right)}{t_1\left(2r_1 + t_1\right)} \qquad (50)$$

This maximum stress cannot exceed the yield strength of copper (σ_y).

$$\sigma_y \geq \frac{P_s\left(r_1^2 + \left(r_1 + t_1\right)^2\right)}{t_1\left(2r_1 + t_1\right)} \qquad (51)$$

Substituting equation (49) into equation (51) gives

$$\sigma_y \geq \frac{\mu_0 t_1\left(r_1^2 + \left(r_1 + t_1\right)^2\right)}{2\left(2r_1 + t_1\right)}\left(J_{c1}k_1\right)^2 \qquad (52)$$

This equation will be rearranged to determine the maximum current density in the stator coils to give (Williamson, "Pulsed," 203)

$$J_{c1(\max)} = \frac{1}{k_1}\sqrt{\frac{2\sigma_y\left(2r_1 + t_1\right)}{\mu_0 t_1\left(r_1^2 + \left(r_1 + t_1\right)^2\right)}} \qquad (53)$$

Now that an equation governing the mechanical stress in the stator coils has been defined, the mechanical stress in the armature can be found. By assuming that the clearance between the armature coils and the stator coils is small, the flux density at the outer surface of the armature is equal to that at the surface of the stator coils (B_{z1} in equation 48). This means that the corresponding radial stress also applies (P_s in equation 49). Therefore, the axial flux density at the inner surface of the armature is approximately

$$B_{z2} = \mu_0\left(J_{c1}k_1t_1 - J_{c2}k_2t_2\right) \qquad (54)$$

Therefore, the radial stress acting on the inner surface of the armature is

$$P_a = \frac{1}{2\mu_0}B_{z2}^2 = \frac{\mu_0}{2}\left[J_{c1}k_1t_2 - J_{c2}k_2t_2\right]^2 \qquad (55)$$

Depending on the relative magnitudes of P_a and P_s, the armature hoop stress varies across it radius with maximum stress appearing on either the inner or outer surfaces.

For the inner surface, $\sigma_y \geq |\sigma_{in}|$,

$$\sigma_{in} = \frac{2P_s r_2^2 - P_a\left[(r_2 - t_2)^2 + r_2^2\right]}{(r_2 - t_2)^2 - r_2^2} \qquad (56)$$

For the outer surface, $\sigma_y \geq |\sigma_{out}|$,

$$\sigma_{out} = \frac{P_s\left(r_2^2 + (r_2 - t_2)^2\right) - 2P_a(r_2 - t_2)^2}{(r_2 - t_3)^3 - r_r^r} \qquad (57)$$

The armature also imparts the accelerating force to the projectile. By assuming that the force is imparted through the cross section of the armature copper, the following relation results

$$P_t\pi\left(r_r^r - (r_r - t_e)^e\right) = \frac{mv}{T} \qquad (58)$$

The axial stress, P_t, must be less than the yield stress of copper. This gives the following inequality (Williamson, "Pulsed," 203-204).

$$\sigma_y \geq \frac{mv}{\pi\left(r_r^r - (r_r - t_2)^2\right)T} \qquad (59)$$

The maximum armature current is assumed to be fixed by the thermal considerations in equation (47).

The maximum stator current is determined by limitations on the hoop stress in the stator coils as in equation (53). Substituting these equations into equation (45) yields

$$(1 + \alpha)mv_{\max}^2 = 2\sqrt{\frac{2\sigma_y(2r_1 + t_1)}{\mu_0 t_1\left(r_1^2 + (r_1 + t_1)^2\right)}}\sqrt{\frac{C_p d\theta}{\rho T}}k_2 l_1 S \tag{60}$$

It is only necessary for the integrity of the armature to be maintained for the duration of the acceleration. Therefore, the time T that it takes for the armature copper to reach its temperature (θ) can be equated to the time it takes for the armature to pass along the barrel.

$$l_1 = \frac{vT}{2} \tag{61}$$

Substituting equation (61) into equation (60), eliminate T yielding (Williamson, "Pulsed," 204).

$$v_{\max} = \left\{\frac{4\sigma_y(2r_1 + t_1)l_1 C_p d\theta k_2^2 S}{u_0 t_1\left(r_1^2 + (r_1 + t_1)^2\right)\rho m^2(1 + \alpha)^2}\right\}^{1/3} \tag{62}$$

Equation (62) can be used to calculate the maximum velocity obtainable from a launcher of given dimensions (r_1, r_2, t_1, t_2, and l_1) for a given projectile mass (m) and armature mass (αm). When this velocity has been determined, the corresponding stator and rotor current densities (J_{c1} and J_{c2}) can be found using equation (53) and equation (47). Once these current densities have been found, the radial stresses produced on the outside of the armature can be calculated from equation (55). Also, the armature hoop stress limits can be checked with equation (56) and equation (57). Finally, the transit time (T) can be found using equation (61), and the axial stress is checked with inequality in equation (59) (Williamson, "Pulsed," 204).

The starting point of the procedure by which performance limits can be determined is assumed to be

Bore (D_b),

Axial stator length (l_1),

Projectile mass (m), and

Thickness for the launch tube or barrel (t_b).

These are the principal independent design variables. The radial clearance between the armature

and bore is small and will be assumed to be 0.5 mm. This will affect the outside radius of the armature (r_2).

$$D_b = 2r_2 + 0.001 \qquad (63)$$

It is also assumed that the stator coils are fit snugly to the outside of the barrel determining the inner radius of the stator (r_1).

$$D_b + 2t_b = 2r_1 \qquad (64)$$

The remaining parameters are the stator thickness (t_1), the armature thickness (t_2), and the overall weight of the armature (αm). By using the equation for the armature mass, the axial length of the armature (l_2) can be found

$$\alpha m = \pi\left(r_2^2 - \left(r_2 - t_2\right)^2\right)k_2 d l_2 \qquad (65)$$

For a given armature weight, the goal is to determine the coil thicknesses (t_1 and t_2) that will produce the maximum projectile velocity. This can be achieved using a standard multivariable optimization

procedure with material constraints are imposed through appropriate penalty functions. In most cases, the maximum velocity corresponds to one or more of the material constraints being met. However, it is difficult to make a blanket statement on which of the various material limits is critical to a particular coilgun. It is certain that relaxation of the material constraints will lead to improvements in the maximum velocity (Williamson, "Pulsed," 204-205). The triple integral, S, given in equation (40) can be evaluated for each set of design variables by means of Gaussian integration. The elliptic integrals that are found in equation (7) can be evaluated using polynomial expansions (Abramowitz).

Chapter 13: Scaling Factors for Linear Induction Launchers

Large caliber electromagnetic launchers require pulsed power sources capable of delivering several tens of megajoules to the breech to accelerate the launch packages. At this time, only a few sources exist that can meet this requirement. If access to one of these sources is not available, meaningful launch experiments can still be performed at a smaller scale.

There are many different criterion for effective scaling. Thermal and electromechanical loading of the solid armature are important parameters in the failure mechanisms of the electrical contact with the rails that induce transition into a hybrid armature. The temperature rise in the armature as a result of Joule heating depends on the course of acceleration in a complex way. Due to the velocity skin effect, the current distribution changes with armature current and also with mass and material properties (Koops, 1).

Scaling relations are derived from the fundamental equations that govern electrothermal and

mechanical behavior of the armature and the stator during the electromagnetic launch. The fundamental equations used include the Maxwell equations, the thermal diffusion equation, the magnetic diffusion equation, and the momentum equation.

In the Maxwell equations, the displacement current is disregarded and only materials with a magnetic susceptibility equal to that of a vacuum are considered.

$$\nabla \times \frac{\overline{B}}{\mu_0} = \overline{J} \qquad (Ampere's \quad Law) \qquad (66)$$

$$\nabla \times \overline{E} = -\frac{\partial \overline{B}}{\partial t} \qquad (Faraday's \quad Law) \qquad (67)$$

$$\overline{J} = \vec{\rho}_e^{-1} \cdot \left[\overline{E} + \overline{v} \times \overline{B} \right] \qquad (Ohm's \quad Law) \qquad (68)$$

From equations (66), (67) and (68), the magnetic diffusion equation can be derived.

$$\nabla \times \left[\vec{\rho}_e \cdot \left(\nabla \times \frac{\overline{B}}{\mu_0} \right) \right] - \nabla \times \left[\overline{v} \times \overline{B} \right] = -\frac{\partial \overline{B}}{\partial t} \qquad (69)$$

The energy balance equation is defined as

$$\nabla \cdot \vec{\kappa} \cdot \nabla T - c_v v \cdot \nabla T = c_v \frac{\partial T}{\partial t} - \overline{J} \cdot \vec{\rho}_e \cdot \overline{J} \qquad (70)$$

The momentum equation reads

$$\nabla \cdot \overline{S} + \overline{J} \times \overline{B} = \rho_m \overline{a} = \rho_m \frac{\partial^2 \overline{s}}{\partial t^2} \qquad (71)$$

In the above equation, the following constants were used. B is the magnetic induction vector, and J is the current density vector. ρ_e is the electrical resistivity tensor, μ_0 is the magnetic susceptibility of a vacuum, and t is the time. E is the vector of the electric field, v is the velocity vector, and ρ_m is the mass density. S is the stress tensor, c_v is the specific heat per unit volume, and κ is the thermal conductivity tensor. T is the temperature, a is the acceleration vector of the launch package, and s is the displacement in the direction of the velocity (Koops, 1-2).

With the fundamental equations now defined, two scaling factors can be introduced: a geometrical scaling factor (g) and a time scaling factor (τ).

$$x' = gx; \qquad y' = gy; \qquad z' = gz$$
$$t' = \tau t \qquad (72)$$

These relations yield the following relations:

$$\nabla' = \frac{\nabla}{g} \qquad and \qquad \frac{\partial}{\partial t} = \frac{1}{\tau}\frac{\partial}{\partial t} \qquad (73)$$

The primed quantities represent the full-scale launcher while the unprimed quantities are from the scaled-down experiment. It should be noted that the time- and positional-dependency of the quantities are not shown (i.e. S(x′,y′,z′,t′) = S′ and S(x,y,z,t) = S).

From equation (69), the scaling relation for the resistivity and velocity can be found

$$\bar{\rho}_e' = \frac{g^2}{\tau}\bar{\rho}_e \qquad and \qquad v' = \frac{g}{\tau}v \qquad (74)$$

Now the scaling factor for the specific heat per unit volume (χ) and the scaling factor for the

temperature (η) are introduced with the following relations:

$$c_v' = \chi c_v \qquad and \qquad T' = \eta T \qquad\qquad (75)$$

Substituting these equations into equation (70) yields

$$\vec{\kappa} = \frac{\chi g^2}{\tau}\vec{\kappa}, \qquad \bar{J}' = \frac{\sqrt{\chi\eta}}{g}\bar{J}, \qquad and \qquad i' = ig\sqrt{\chi\eta} \qquad\qquad (76)$$

By now substituting equation (76) into (66) gives

$$\bar{B}' = \bar{B}\sqrt{\chi\eta} \qquad\qquad (77)$$

Using the momentum equation in (71) now yields

$$\rho_m' = \frac{\tau^2\chi\eta}{g^2}\rho_m \qquad and \qquad \bar{S}' = \chi\eta\bar{S} \qquad\qquad (78)$$

Important launch parameters like acceleration, velocity, and displacement also need to be scaled.

$$\bar{a}' = \frac{g}{\tau^2}\bar{a}, \qquad \bar{v}' = \frac{g}{\tau}\bar{v}, \qquad and \qquad \bar{s}' = g\bar{s} \qquad\qquad (79)$$

The consequence of the scaled acceleration is that the mass of the total launch package (m) must also be scaled.

$$m' = g\tau^2\chi\eta m \qquad (80)$$

The mass density (ρ_m) can be considered as the average mass density of the launch package (Koops, 2).

Applying the scaling relations to the launch parameters can draw some interesting conclusions. When the inductance gradient of the accelerator (inductance per unit length) is considered as a lumped parameter, it will be invariant under scaling (i.e. $L' = L$) (Grover). It should be noted that the length of the accelerator in the small-scale experiment could be g times smaller than the full-scale version. The kinetic energy is independent of the time scaling factor τ (i.e. $E_{kin}' = g^3\chi\eta E_{kin}$).

Another very useful aspect of the scaling relations is that three parameters that are used to characterize the quality of the launch process are invariant under the scaling. These are the launch efficiency (η_{launch}), the total efficiency (η_{total}), and the armature figure of merit (FOM).

$$\eta_{launch}' = \eta_{launch} = \frac{kinetic \quad energy \quad of \quad the \quad launch \quad package}{energy \quad input \quad at \quad the \quad breech} \tag{81}$$

$$\eta_{total}' = \eta_{total} = \frac{kinetic \quad energy \quad of \quad the \quad launch \quad package}{energy \quad stored \quad in \quad the \quad pulsed \quad power \quad source} \tag{82}$$

$$FOM' = FOM = \frac{kinetic \quad energy \quad of \quad the \quad launch \quad package}{energy \quad dissipated \quad in \quad the \quad armature} \tag{83}$$

The electrothermal action absorbed by the armature scales to (Koops, 3)

$$A' = g^2 \tau \chi \eta A \tag{84}$$

It was shown that certain aspects of large caliber armatures during electromagnetic launch could be studied at smaller scales by applying certain scaling relations. These relations are derived from

the fundamental equations describing the electromagnetic launch process. There are four scaling factors: g for geometrical scaling, τ for time scaling, χ for scaling of the specific heat per unit volume, and η for temperature scaling. There are critical design parameters that are invariant under scaling including the launch efficiency, the total efficiency, and the armature figure of merit (Koops, 8).

Chapter 14: Transitions in a Multi-Section Launcher

In linear induction launchers, the barrel is divided into sections. Each section is energized in polyphase fashion by discharging a capacitor bank through the drive coils and maintains a constant pole pitch. The frequency of the currents in the drive coils and the capacitor voltages progressively increase from the breech of the barrel to its muzzle. When the projectile moves from one section to another, the frequency of the currents in the drive coils increases. Therefore the velocity of the propelling traveling waves increases (Lu, 493).

When the first section is energized, the projectile is at a standstill with an initial slight displacement in the direction of motion. The propelling force is produced by only the transformer action before the traveling wave builds up (Bondaletov, 210-215). After this traveling waves builds up, the sleeve current is mostly motion-induced causing the wave to drag the projectile forward.

The energization of the second section is different from that of the first section because the projectile now has acquired a significant velocity. Whether this motion attenuates the effect of the backward travelling wave that is generated by the single-phasing depends on the position of the sleeve inside the second section and also depends on the initial velocity of the of the projectile when the second section is fired. Either the initial position of the sleeve or a pre-set time delay can be used to determine the moment to energize the second section of the launcher in order to get maximum muzzle velocity (Lu, 493).

A number of computer models have been developed to study the electromechanical behavior of linear induction launchers. During the motion, the sleeve is primarily subjected to accelerating forces in the axial direction, and in a coaxial situation the radial forces have no resultant. Nevertheless, deviations from this ideal situation can cause an uneven distribution of radial forces. Also, components of motions in transverse directions can result from the action of these uneven radial forces as well as result

in oscillations around the sleeve mass center. Contact between the sleeve and the barrel can result which will cause degraded performance of the launcher and may damage the launch tube. The forces acting on the sleeve can assume the characteristics of a restoring force in the opposite direction of the deviation that will support the projectile to avoid contacts with the barrel (Wang, 195).

During the transitions between sections, a possible mismatch of the currents in the sleeve with respect to the currents in the drive coils can cause forces that will tend to increase the deviation from the coaxial condition. Also, there are other conditions that can cause contact between the sleeve and the barrel can occur during the transition between sections. When the sleeve has partially left the first section, the thrust force is mainly concentrated towards the rear of the sleeve. If the axis of the sleeve is not aligned with the axis of the barrel, then a momentum acts on the sleeve that can increase the differences in the alignment of the axes (Musolino, "3-D," 2).

When the coaxial alignment in a linear induction launcher is broken, six degrees of freedom are required to fully describe the motion of the sleeve; however, only three degrees of freedom are used in the following model: x and θ are used to describe the transverse motion of the sleeve and z coincides with the axis of the barrel.

Figure 23: Coordinate System

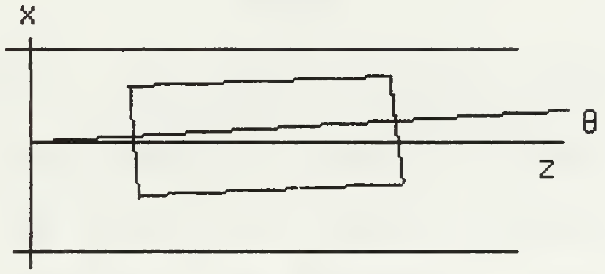

In Figure (23) above, x represents the position of the mass center of the sleeve and θ denotes the angle of rotation of the sleeve axis with respect to the barrel axis. It is assumed that the transverse motion is the y-axis has no component, no rotation around the x-axis and no spinning is present (Musolino, "3-D," 2-3). The electromechanical analysis is performed by means of a numerical method (Esposito).

Figure 24: Elementary Volumes

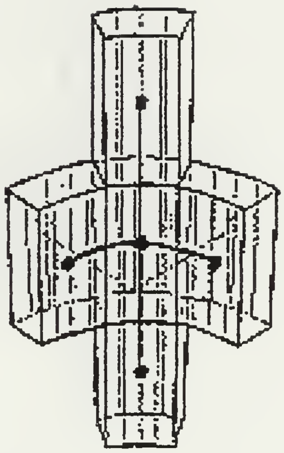

Consider a cylindrical aluminum sleeve that is subdivided into sectors as shown in Figure (24). By connecting the centers of nearby elements, a three-dimensional grid can be obtained. New elementary conductive elements are associated to the segments of the grid. See Figure (25). Only the components of the current density parallel to the associated segment have any value inside the new volume elements where the current is assumed to be uniformly distributed.

Figure 25: Elementary conductive volumes

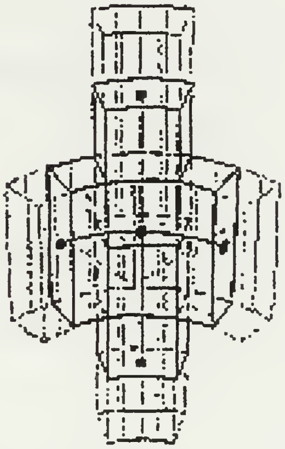

The fields and potentials produced by these currents are evaluated by integration over the elementary volumes.

$$\overline{A}_k(t) = \frac{\mu_0}{4\pi}\sum_{j=1}^{N_s}\overline{J}_j(t)\int_{V_{s,j}}\frac{1}{|x_k - x'|}\,d^3x' \qquad (85)$$

$$\overline{B}_k(t) = \nabla\times\overline{A}_k(t) \qquad (86)$$

Ohm's law inside every conductive volume is defined as

$$\rho_k\overline{J}_k(t) = -\nabla V_k(t) - \frac{\partial\overline{A}_k(t)}{\partial t} + \overline{v}_k(t)\times\overline{B}_k(t) \qquad (87)$$

A_k is the magnetic vector potential in the *k*-th volume. $-\nabla V_k$ is the irrotational component of the

electric field, v_k is the velocity relative to the flux density B_k, and J_k is the current density.

Next the expressions of the fields and potentials as a function of the currents in the systems are substituted into Ohm's law, and the result is projected along the direction of the current in the *k*-th volume. Averaging the result over the surface S_k yields

$$R_k I_k(t) + \sum_{j=1}^{N_i} L_{jk} \frac{d}{dt} I_j(t) + \sum_{j=1}^{N_i} K_{jk} I_j(t) = U_k(t) \tag{88}$$

U_k is the potential drop, R_k is the resistance in the *k*-th volume, L_{jk} is the induction coefficient between the *j*-th and the *k*-th volume, and K_{jk} represents the electromotive force due to the relative motion of the *k*-th element with respect to the *j*-th one (Musolino, "3-D", 3).

These coefficients are dependent on the relative motion of the volumes and need to be continually updated during the motion of the projectile with respect to the barrel. The analytical expressions of the fields and potentials produced by the cylindrical

sectors can be quickly evaluated by means of Gaussian quadrature formulas.

Figure 26: Electric branch of the equivalent network

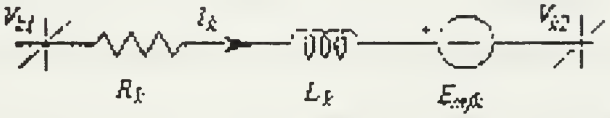

Equation (88) represents the electric equilibrium equation of the branch of a network shown above in Figure (26) where a resistor, an inductor that is coupled with the inductors of the other branches in the network, and a voltage-controlled generator are all present. The E_{mfk} generator is controlled by the currents in the branches of the network representing the moving elements with respect to the *k*-th volume.

Once the current distributions in the sleeve are known, the calculation of the thrust force can be performed using the Laplace formula.

$$\overline{f}_k(t) = \int_{\Gamma_k} \overline{J}_k(t) \times \overline{B}_k(t) dv \qquad (89)$$

J_k is the current density in the *k*-th element, and B_k is the flux density (Musolino, "3-D," 3-4).

The results of these force equations and of the torque have to be introduced into the motion equations. Also if the sleeve comes into contact to the barrel, the contribution of the restoring force must be taken into account. It is assumed that there is an elastic deformation of the barrel and that the restoring forces per unit length are proportional to the local displacement (Shokair). Also, a drag force, which is proportional to the restoring force, acts on the sleeve.

A single-step time marching algorithm is used for the resolution of the differential equations expressing the electric equilibrium of the equivalent network. The magnetic fields can be calculated and then the magnetic forces acting on the elementary volume of the sleeve can also be calculated. By summing the forces on all of the volumes, the total thrust force is found (Musolino, "3-D," 4). The entire procedure can be summarized in five steps.

Initialize the currents of the equivalent electric network at time $t=t_0$: $\underline{I}(t_0)=\underline{I}_0$. Also, initialize the position, the velocity, and the time step Δt. Set $F_0=0$, $\tau_0=0$, and $n=1$.

Next, evaluate the matrices of the self and mutual inductance ($\underline{\underline{L}}_{jk}$) and of the motional terms ($\underline{\underline{K}}_{jk}$). Also, the equilibrium equations of the network need to be assembled by means of mesh analysis.

Now the currents in the equivalent electric network can be calculated using a single step time marching algorithm:

$$\underline{I}_n = \underline{I}_{n-1} + \underline{\beta}_n \Delta t \qquad (90)$$

$$\text{where} \qquad \underline{\beta}_n = \left(\underline{\underline{L}}_n + \frac{2}{3} \Delta t \left(\underline{\underline{R}}_n + \underline{\underline{K}}_n \right) \right)^{-1} \left(\underline{U}_n - \left(\underline{\underline{R}}_n + \underline{\underline{K}}_n \right) \underline{I}_{n-1} \right)$$

From the currents that have been calculated, the force F_n and the torque τ_n acting on the sleeve can be evaluated. Where M is the total mass and G is the moment of inertia with respect to a transverse axis, the acceleration, the velocity, the position of the mass and the angle of rotation with respect to the axis of the barrel can be calculated as follows:

$$\bar{a}_n = \frac{\bar{F}_n + \bar{F}_{n-1}}{2M} \qquad (91)$$

$$\bar{v}_n = \bar{v}_{n-1} + \bar{a}_n \Delta t \qquad (92)$$

$$\bar{x}_n = \bar{x}_{n-1} + \frac{\bar{v}_n + \bar{v}_{n-1}}{2} \Delta t \qquad (93)$$

$$\dot{\omega}_n = \frac{\tau_n + \tau_{n-1}}{2G} \qquad (94)$$

$$\omega_n = \omega_{n-1} + \dot{\omega}_n \Delta t \qquad (95)$$

$$\theta_n = \theta_{n-1} + \frac{\omega_n + \omega_{n-1}}{2} \Delta t \qquad (96)$$

The last step is to increase the value of n (n=n+1) and repeat starting at the second step.

These steps assume that the displacements during each time step (Δt) are small enough so that the elements $\underline{\underline{L}}_{jk}$ and $\underline{\underline{K}}_{jk}$ remain reasonably constant. This condition can be used to control the time step as the velocity increases (Musolino, "3-D," 4-5).

Figure 27: Two section linear induction launcher

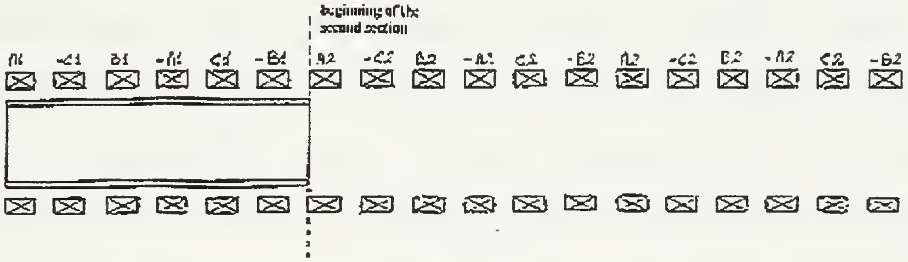

Figure (27) above shows a two-section linear induction launcher that this model was used to analyze. The first section consists of six equally sized coils that are excited by a three-phase set of currents at a constant frequency. Each coil has an inner radius of 2.75 cm, an outer radius of 3.5 cm and a height of 1.5 cm. The space between adjacent coils is 1.0 cm. The second section is composed of twelve coils with the same dimensions and spacing as the first section. The frequencies of the exciting generators are 1250 Hz in the first section and 2500 Hz in the second section. Each coil is energized at the instant of zero current crossing.

The sleeve, or projectile, is an aluminum cylinder of an inner radius of 2.0 cm, an outer radius of 2.5 cm, and a length of 15 cm. The sleeve is subdivided into 15 equal parts along the axial direction, and each resulting ring is further divided in 12 sectors. The initial position of the sleeve inside the first section is characterized by a displacement of 2.9 mm between its axis and the axis of the barrel with both axes being parallel.

In this multi-section launcher, only the section of the barrel in which the sleeve is located is excited. This experiment investigated the behavior of the launcher with different instants of the firing of the second section. These instants were chosen with the leftmost position of the sleeve with respect to the beginning of the second section. The simulations were performed with displacements of -3.5, -2.5, -1.5, -0.5, 0.5, 1.5, 2.5, and 3.5 cm (Musolino, "3-D," 6).

Figure 28: Velocity profile for different values of the initial position in the second section

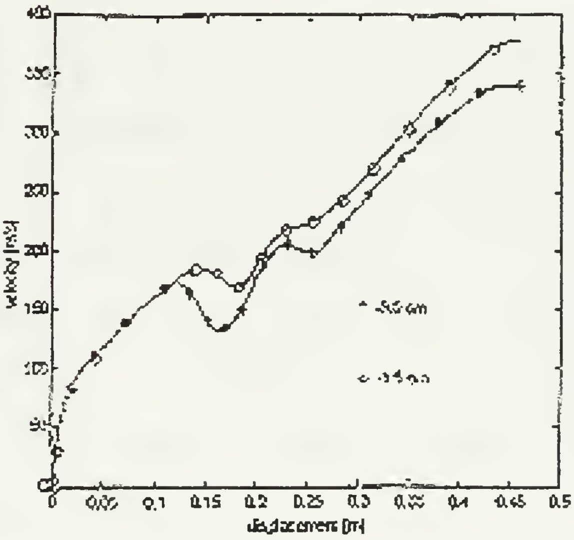

Figure 29: Velocity profile for different values of the initial position in the second section

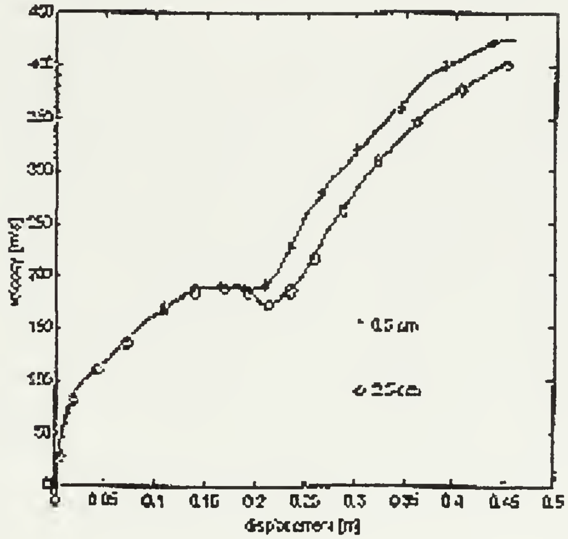

Figures (28) and (29) above show the velocity profile for different displacements. The highest muzzle velocity was obtained at a displacement of 0.5 cm. For the other displacements, the figure shows a braking effect at the transition point. This is possibly due to a mismatch of the induced sleeve currents. This braking effect lowers as the firing position moves towards the beginning of the second section (Musolino, "3-D," 5-7).

This analysis of the motion in a two-section linear induction launcher has shown that the choice of

the fire timing of the second section can greatly influence the performance of the muzzle velocity.

Chapter 15: Conclusions of Electromagnetic Theory

In this section, many aspects of electromagnetic launchers were discussed. The differences in the railgun and the coilgun were explored. Not only were the conceptual differences noted but also how they perform. It was shown that the railgun is a simpler design than the coilgun and is also able to be made in smaller sizes. On the other hand, the coilgun is more complex but also more efficient and does not need the sliding contacts that a railgun does.

Next, the stresses on electromagnetic launchers were discussed. These were used to develop an ideal model of a coilgun. In this complex analysis, the effects of the gap size and the thickness of the moving conductor of the barrel and of the projectile were shown. This analysis also showed the relations between the sheet currents of the barrel and of the projectile.

Then, the limitations of a coilgun were discussed. This analysis showed by establishing certain design constraints that many performance

characteristics of the coilgun can be found. Then, the optimization of the coilgun can be achieved by adjusting certain variable limits. After that, scaling relation were established. These relations can be used to design more cost effective prototype of larger electromagnetic launchers.

Finally, the reactions at transition points between sections were explored. This shows that the exact timing of section energization needs to be determined on an individual basis to achieve optimization.

All of the investigation establishes all of the necessary theory for the design of an electromagnetic launcher.

SECTION IV: POWER SYSTEMS

Section IV is a review of the various power systems available for linear induction launchers. Chapter 16 is a general overview of the different power systems. Chapter 17 is a more in-depth review of the pulse forming network.

Chapter 16: Pulsed Power Systems

Railguns and coilguns rely on pure electromagnetic forces to accelerate projectiles to high velocities. Therefore, substantial energy input is needed at the breech of the gun for each shot. The required breech input energy is derived from the mission requirements of the gun including efficiency and muzzle velocity. In addition to the energy pulse, it is necessary to provide average power to the electrical system at a rate that matches the firing rate of the electromagnetic gun. To supply this power, a prime mover (e.g. internal combustion engine, gas turbine, or nuclear reactor) and a generator with a transformer/rectifier must provide electrical power to the energy storage system (McNab, "Pulsed," 453-454).

From the earliest days of electric gun research, the pulse power systems was recognized as one of the most critical components for successful development. Achieving high levels of energy density (several MJ/kg) in a system that stores and transfers

electrical energy is very difficult. However, there are many options for such systems.

One of the earliest energy storage systems used in electromagnetic launchers is a capacitor bank. Capacitor banks offer a few advantages including the wide availability of components and their low costs in small sizes. Simple experiments were conducted where banks were used with undamped oscillating output currents whose characteristic time period is matched to the transit time of the projectile. These experiments did usually result in substantial current variations and very non-uniform acceleration. In some cases, the averaged fluctuating current has been accepted as an inexpensive way to undertake experiments. The better arrangement is to crowbar the circuit after the current has reached it peak value that will extend the high current portion of the output pulse (McNab, "Pulsed," 455-456).

Despite the crowbarring of a single capacitor bank, current drops can cause inefficiencies in a long launch. Therefore, a preferable design is the subdivision of the capacitor into separate independently triggered modules that is called pulse

forming networks. Pulse forming networks can provide a flat-topped pulse by using several modules that are separately triggered to match the transit time of the projectile of the barrel.

To get the desired high initial acceleration, a high energy module is initially fired and then followed by the subsequent discharge of smaller modules. Because the projectile is travelling at higher velocities further down the barrel, the later modules generally have smaller inductors in series with the capacitor modules to achieve faster current rise times (McNab, "Experiments," 338-343).

While pulse forming network can efficiently transfer the stored energy to the launcher, they do have some complications. One problem is that the output switches that connect each stage to the load must prevent current from later modules from being partially discharged back into earlier modules (Augsburger, 10-15). If this discharge is not taken into account, considerable amount of stored energy could be lost before it reaches the barrel.

The single largest contributor to the total system size and mass in a pulse forming network is the

capacitors in which the energy is stored. The energy stored in a dielectric is proportional to the dielectric constant (ε_r). For many years, the standards in the capacitor industry were capacitors that used paper dielectrics with foil electrodes. Now, plastic films such as polyethylene, polypropylene, and polyvinylidene fluoride provide better performance. Polyethylene has a dielectric constant of 2.1 and a stored energy density of 0.37 MJ/m^3. Polypropylene has a dielectric constant of 3.25 and a stored energy density of 1.3 MJ/m^3. Polyvinylidene fluoride has a dielectric constant of 10 and a stored energy density of 7 MJ/m^3. While the polyethylene and polypropylene provide adequate dielectrics, the newer polyvinylidene fluoride is much better. The only problem with the polyvinylidene fluoride is that the energy density is non-linear so it is more difficult to characterize, less efficient, and more difficult to integrate into a system (McNab, "Pulsed," 456). Therefore until new materials are developed, it can be concluded that pulse forming networks are not a feasible energy storage device for linear inductive launchers.

One alternative to capacitors as an energy storage device is the use of homopolar generators. Unfortunately, homopolar generators deliver a low voltage so a pulse compression stage must be added where the energy is transferred into an inductor for temporary storage as magnetic energy. Getting the energy into the inductor is simple but getting the energy from the inductor to the launcher requires an opening switch. This opening switch needs to be able to carry a high current during inductor charging and also needs to be able to open quickly against the current when the transfer is required. It is the need for an opening switch and storage inductor that makes the homopolar generator an impractical energy storage device of linear induction launchers (McNab, "Pulsed," 457).

Chapter 17: Pulse Forming Networks

The power source needed for linear induction launchers must be capable of delivering high current pulses for a long duration. The L-C ladder network, or pulse forming network, is able to meet the demands of the linear induction launcher. One way to optimize an L-C ladder to adopt time domain procedures for a nonlinear load. This procedure requires a considerable amount of simulations. Another way to optimize the L-C network is to develop simple mathematical relations between the rise time, the duration, and the magnitude of the pulse. These relations will allow the values of the capacitance and inductance of the branches to be determined (Di Capua, 554-559).

In order to develop the equations necessary, several design parameters must be given. These include the total pulse duration(τ), the pulse rise time(τ_r), the pulse working time(τ_p), and the pulse fall time(τ_f). From these values the ratio between the rise time and the total time (Γ) can be found. Also, the

initial charged voltage (V_0) must be given. Also given will be the required pulse current amplitude (I_d), the required current delivered to the load (i_d), and the real current delivered to the load (i_1).

To begin the design, it is assumed that the electromagnetic launcher is represented by a linear resistor (R_1). The input data for the design procedure is the pulse duration, the rise time, the amplitude of the current, the number of sections of the L-C ladder network and the equivalent resistance of the launcher. See Figures (30) and (31) below (Musolino, "Pulse," 480).

Figure 30: Required Trapezoidal Current Pulse

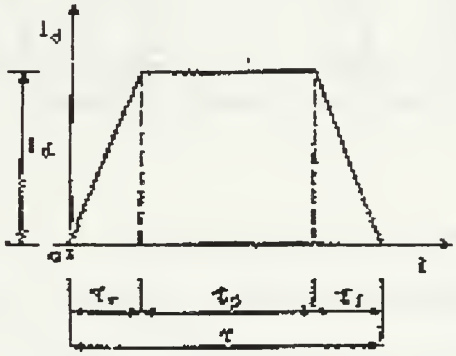

Figure 31: Lossless L-C ladder network.

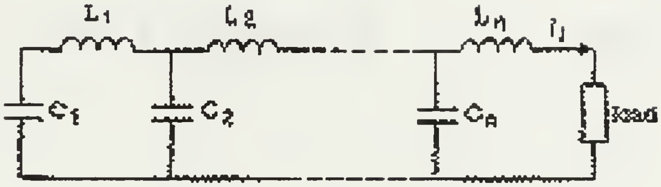

Taking the input data and applying Guillemin's theory, the values of the capacitances and inductances of a network with parallel branches can be determined (Guillemin). See Figure (32) below.

Figure 32: Auxiliary Parallel Network

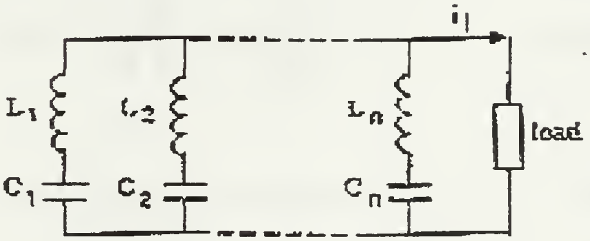

Although it is impossible to generate an ideal rectangular pulse from a lumped parameter network, it is possible to design a network that delivers a pulse with a very short rise and fall time.

Consider the Fourier series for a trapezoid wave.

$$i(t) = b_0 + \sum_{k=1}^{\infty} b_k \sin \frac{k\pi t}{\tau} \tag{98}$$

$$\textit{where} \qquad b_0 = \frac{1}{2\tau} \int_0^{\tau} i(t)dt$$

$$\textit{and} \qquad b_k = \frac{1}{2\tau} \int_0^{\tau} i(t) \sin \frac{k\pi t}{\tau}\, dt \tag{99}$$

The current that each branch delivers to the load is as follows.

$$i_k(t) = V_0 \sqrt{\frac{C_k}{L_k}} \sin \frac{-t}{\sqrt{L_k C_k}} \tag{100}$$

From a comparison between equation (100) and the coefficients of the Fourier series, the values of L_k and C_k can be found.

$$L_k = \frac{V_0 \tau}{4I_d - \dfrac{\sin k\pi\alpha}{k\pi\alpha}} \tag{101}$$

$$C_k = \frac{4I_d \tau \sin k\pi\alpha}{k^3 \pi^3 V_0 \alpha} \tag{102}$$

These equations define a network of a given number of L-C sections that resonate at a frequency of k/2τ arranged in parallel (Musolino, "Pulse," 481). The inductances have an appreciably distributed capacitance that will actually shunt them and tend to spoil the pulse shape. Also, the condensers have a wide range of values which makes manufacturing difficult and expensive (Glasoe).

By taking the auxiliary network, an equivalent ladder network can be found by comparing the output impendences of the networks. The impedance of the parallel branch network can be found where n is the number of the branches in parallel.

$$Z_{par} = \frac{\prod_{k=1}^{n}\left(1 + s^2 L_k C_k\right)}{\sum_{k=1}^{n} sC_k \prod_{\substack{j=1 \\ j\neq k}}^{n}\left(1 + s^2 L_j C_k\right)} \qquad (103)$$

The impedance of the ladder network can be written by making use of a continued-fraction expansion of the reactance and the admittance. The expression can be derived from equation (103) by dividing the numerator by the denominator. This will

yield L_n. Then inverting the remaining fraction and dividing again will yield C_n and so on until the expression is found.

$$Z_{lad} = sL_n + \cfrac{1}{sC_n + \cfrac{1}{sL_{n-1} + \cfrac{1}{sC_{n-1} + \cdots + \cfrac{1}{sC_2 + \cfrac{1}{sL_1 + \cfrac{1}{sC_1}}}}}} \tag{104}$$

The above ladder network will be completed with the addition of parasitic parameters. The parameter values are considered to be in proportion to its corresponding elements. There are usually a parasitic inductance (L_C) and resistance (R_C) in series with the capacitors and a parasitic resistance (R_L) in series with the inductor. The parasitic values are usually given by the manufacturers and can be controlled. See Figure (33) below for a complete picture (Musolino, "Pulse," 481).

Figure 33: Complete L-C Ladder Network

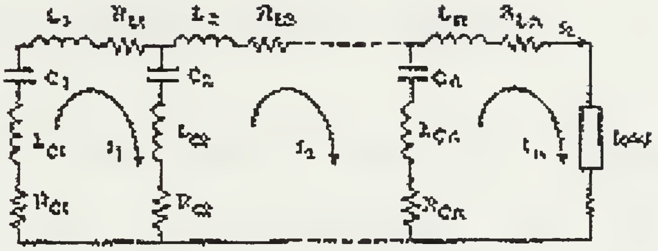

By using a minimum square deviation performance index, the complete pulse forming network can be optimized as shown below where W_j are suitable weights, $i_d(t)$ is the required current, i_1 is the obtained current, and m is a suitably large natural numbers.

$$Q = \sum_{j=0}^{m} W_j \int_{j\tau}^{(j+1)\tau} \left[i_d(t) - i_1(t) \right]^2 dt \tag{105}$$

The loop currents in Figure (33) can be expressed in Laplace's form.

$$\begin{aligned} i_j = {} & \frac{\left(s^2 C_j C_{j+1} L_{C_{j+1}} + s C_j C_{j+1} R_{C_{j+1}} + C_j\right) den(i_{j-1}) i_{J+1}}{\left[s^2 C_j C_{j+1}\left(L_j + L_{C_j} + L_{C_{j+1}}\right) + s C_j C_{j+1}\left(R_{L_j} + R_{C_j} + R_{C_{j+1}}\right) + C_j + C_{j+1}\right]} \cdot \\ & \frac{1}{den(i_{j-1}) - \left[s^2 C_j C_{j+1} L_{C_j} + s C_j C_{j+1} R_{C_j} + C_{j+1}\right] num(i_{j-1})} \end{aligned} \tag{106}$$

$$i_n = \frac{V_0 C_n den(i_{j-1})}{\left[s^2 C_n\left(L_n + L_{C_n}\right) + sC_n\left(R_{L_n} + R_{C_n} + R_{load}\right) + 1\right]} \cdot \frac{1}{den(i_{n-1}) - \left[s^2 C_n L_{C_n} + sC_n R_{C_n} + 1\right] num(i_{n-1})} \tag{107}$$

Num(i) and den(i) are the numerator and denominator of the expression of the current respectfully where num(i_0)=0 and den(i_0)=1. V_0 is the initial charged voltage (Musolino, "Pulse," 481-482).

From the knowledge of the loop currents, the currents in the branches of the network can be found. The current in the inductor of the horizontal branches is equal to the corresponding loop current. Also, the current in the capacitor of the j-th vertical branch is the same as the difference between i_j and i_{j-1}. The expressions of the currents versus time are obtained from the inverse Laplace transforms of equations (106) and (107). In particular, equation (107) becomes

$$i_l = \sum_{i=1}^{n} 2\left|I_i\right| \cos\left(IM_i t + PH_i\right) e^{RE_i t} \tag{108}$$

Re_i and Im_i are the real and imaginary parts of the I-th pole. I_i is the module of the I-th residue of the partial fraction expansion of equation (107). Ph_i

is the phase of the I-th residue of the same partial fraction.

Also, the integral in equation (105) can be solved analytically (Musolino, "Pulse," 482).

$$\int_0^{\Gamma} \left[i_d(t) - i_l(t)\right]^2 dt = \sum_{i=1}^{n} 2|I_i|^2 e^{2RE_i t} \left[\frac{1}{RE_i} + \frac{A}{RE_i^2 + IM_i^2}\right]_0^{\Gamma}$$

$$+\sum_{i=1}^{n-1} \sum_{j=i+1}^{n} 4|I_i||I_j| e^{Bt} \left[\frac{C}{D} + \frac{E}{F}\right]_0^{\Gamma} + I_d^2 \tau\left(1 - \frac{4}{3}\alpha\right)$$

$$-\sum_{i=1}^{n} 4\frac{I_d}{\tau_r}|I_i| \left[\frac{G\left(H + j\frac{IM_i}{RE_i}\right) + e^{RE_i t}\frac{IM_i^2 K}{RE_i^2 M} - IM_i\frac{L}{M}}{M}\right]_0^{\tau_r}$$

$$-\sum_{i=1}^{n} 4|I_i||I_j| e^{RE_i t} \left[\frac{K}{RE_i^2 + IM_i^2}\right]_{\tau_r}^{\tau_q} + \sum_{i=1}^{n} \frac{4}{\alpha} I_d |I_j| e^{RE_i t} \left[\frac{K}{RE_i^2 + IM_i^2}\right]_{\tau_r}^{\tau_q}$$

$$-\sum_{i=1}^{n} 4|I_i| \frac{I_d}{\tau_r} \left[\frac{G\left(H + j\frac{IM_i}{RE_i}\right) + e^{RE_i t}\frac{IM_i^2 K}{RE_i^2 M} - IM_i\frac{L}{M}}{M}\right]_{\tau_q}^{\tau}$$

(109)

where

$$A = RE_i \cos(2IM_i t + 2PH_i) + IM_i \sin(2IM_i t + 2PH_i)$$

$$B = RE_i + RE_j$$

$$C = (RE_i + RE_j)\cos((IM_i - IM_j)t + PH_i - PH_j) + (IM_i - IM_j)\sin((IM_i - IM_j)t + PH_i - PH_j)$$

$$D = (RE_i + RE_j)^2 + (IM_i - IM_j)^2$$

$$E = (RE_i + RE_j)\cos((IM_i + IM_j)t + PH_i + PH_j) + (IM_i + IM_j)\sin((IM_i + IM_j)t + PH_i + PH_j)$$

$$F = (RE_i + RE_j)^2 + (IM_i + IM_j)^2$$

$$G = e^{RE_i t}(RE_i t - 1)$$

$$H = \cos(IM_i t + PH_i)$$

$$J = \sin(IM_i t + PH_i)$$

$$K = RE_i \cos(IM_i t + PH_i) + IM_i \sin(IM_i t + PH_i)$$

$$L = RE_i \sin(IM_i t + PH_i) - IM_i \cos(IM_i t + PH_i)$$

$$M = (RE_i)^2 + (IM_i)^2$$

$$\tau_q = \tau_r + \tau_p$$

With the above equations, the optimization of the pulse formed network defined in equations (101), (102), (103), and (104) can be completed. This pulse forming network should be able to act as the power supply of an electromagnetic launcher when given the correct design parameters (Musolino, "Pulse, 482-483).

SECTION V: THE ELECTROMAGNETIC GUN EXPERIMENT

Section V discusses an experiment to test the precision of an electromagnetic gun. Chapter 18 describes the theory behind the experiment. Chapter 19 is a review of the experiment itself.

Chapter 18: Electromagnetic Gun Diagnostic Theory

A magnetic field probe is a small conductive loop that will produce an output voltage proportional to the time rate of change of the magnetic flux linking the loop. In the past two decades, magnetic probes have been one of the primary diagnostic tools used to assess the performance of railgun-type electromagnetic launchers (Parker, 487).

Figure 34: Schematic drawing of plasma-armature railgun.

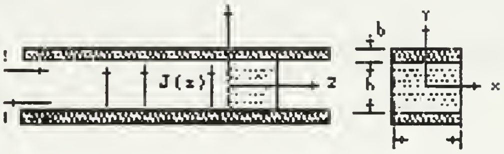

The intrinsic property of magnetic field probes is that they are sensitive only to the component of the magnetic field perpendicular to the plane of the loop. The magnetic field probes do not respond to the fields parallel to the plane of the loop. This can be expressed mathematically where the voltage generated

by the loop is in terms of the loop geometry (Jamison, 403-406).

$$V_m = NA \frac{d}{dt}\left(\hat{n} \cdot \overline{B}\right) \qquad (110)$$

The number of turns is represented by (n) and the area of the loop is (A). The dependence on orientation is introduced through the unit vector (n) that is normal to the plane of the loop.

By substituting the Biot-Savart expression, an expression for the output voltage can be found in terms of the source current (j) and the vector distance (r) between the source current and the measurement point.

$$V_m = \frac{\mu_0 NA}{4\pi} \frac{d}{dt} \int \frac{\left(\hat{n} \times \vec{j}\right) \cdot \vec{r}}{\left|\vec{r}\right|^3} dV \qquad (111)$$

Because the vector product (n x j) is equal to zero for (j || n), this shows that the magnetic loop measures all of the currents except for those parallel to the loop normal (Parker, 487-488).

Figure 35: Geometry for calculating the armature current probe response in the current filament approximation. (Parker, 489)

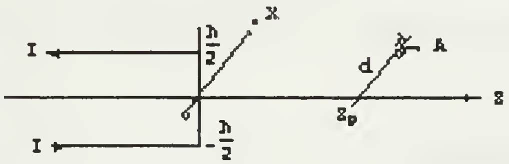

The response of a magnetic field probe to the currents in a railgun can be analytically for only a few simple current distributions. Two of the more common assumptions are the current filament model shown in Figure (34) and the current sheet model. The current filament model gives a good estimation of the magnetic field when (d >> h/2) and (d >> w/2). The value of (h) is the bore height plus a fraction of the rail thickness (~30%). The value (w) represents the width of the discharge and (d) is the distance of the probe from the z-axis in the direction of the x-axis. In general, the current filament model is adequate for estimating the probe signal strength and for investigating the probe response function in the limit $d \rightarrow \infty$.

When the probe spacing becomes comparable to h and/or w, then the current sheet model gives a better approximation for the magnetic field. Both models assume a current distribution that is singular in the axial direction.

The coordinate system and probe geometry for armature probe calculations are shown in Figure (35). This figure illustrates the current filament model. The current sheet model follows by spreading the current uniformly in the x direction over the interval $-w/2 \le x \le w/2$. The primary calculation presented is the flux linking the probe coil. This is the signal that is generated by integrating the coil output voltage. It is assumed that the entire plasma moves at a common velocity: $v(z,t) = v(t)$. Also, it is assumed that the current does not vary with time: $\partial I/\partial t = 0$. These will always be held true if the input current is constant (Parker, 487-488).

In the following equations, the number of turns is given as N, A is the area of the coil, $\phi_p^A(t)$ is the flux linking an armature probe at location z_p, and $d\phi/dt$ denotes the direct output signal. The following approximations at located at $x = d$, $y = 0$, and $z = z_p$.

Current Filament Approximation

$$\phi_p^A(t) = \frac{\mu_0 NAI}{4\pi}\left(\frac{d}{d^2 + z_p^2}\right)\frac{h}{\sqrt{d^2 + z_p^2 + (h/2)^2}} \tag{110}$$

$$\phi_p^A(t) = \frac{3\mu_0 NAIv}{4\pi}\,\frac{d}{\left(d^2 + z_p^2\right)^2}\,\frac{z_p h\left[z_p^2 + d^2 + \frac{2}{3}(h/2)^2\right]}{\left(z_p^2 + d^2 + (h/2)^2\right)^{3/2}} \tag{111}$$

Current Sheet Approximation

$$\phi_p^A(t) = \frac{\mu_0 NAI}{4\pi w}\ln\left[\begin{array}{l}\dfrac{\sqrt{(d + w/2)^2 + (h/2)^2 + z_p^2} - (h/2)}{\sqrt{(d + w/2)^2 + (h/2)^2 + z_p^2} + (h/2)}\\ \bullet\,\dfrac{\sqrt{(d - w/2)^2 + (h/2)^2 + z_p^2} + (h/2)}{\sqrt{(d - w/2)^2 + (h/2)^2 + z_p^2} - (h/2)}\end{array}\right] \tag{112}$$

$$\phi_p^A(t) = \frac{\mu_0 NAI}{4\pi w} z_p h\left[\begin{array}{l}\dfrac{1}{\left[(d + w/2)^2 + z_p^2\right]\sqrt{(d + w/2)^2 + z_p^2 + (h/2)^2}}\\ -\dfrac{1}{\left[(d - w/2)^2 + z_p^2\right]\sqrt{(d - w/2)^2 + z_p^2 + (h/2)^2}}\end{array}\right] \tag{113}$$

These equations can be used to describe various probe responses to an armature whose entire current is concentrated at a single axial location. These formulas can be used as the stating point for a calculation of the probe response to an armature with a current distribution $J_y(z)$. An example is to calculate the armature current probe response in the current filament approximation by using equation (110) to find the response to a current element located at a point z (Parker, 498-499).

$$d\phi_p^A(t) = \frac{\mu_0 NA}{4\pi} J_y(z)dz \frac{d}{d^2 + \left(z_p - z\right)^2} \bullet \frac{h}{\sqrt{\left(z_p - z\right)^2 + d^2 + \left(h / 2\right)^2}} \tag{114}$$

Chapter 19: Electromagnetic Gun Experimentation

As has been discussed earlier, magnetic field probes can be used to assess the performance of electromagnetic launchers. The output voltage of the probes is proportional to the time rate of change of the magnetic flux. By measuring the output voltage produced by the magnetic field loops, the velocity of the armature can be found as the exact location of the loops are know.

To demonstrate this theory, the B-dot plots were used to analyze the plasma armature motion of the bench test railgun (BTR). B-dot is the common name given to the rate of change of the magnetic flux density (i.e. dB/dt). These plots show a comparison of the B-dots versus time. The bench test railgun was designed as a plasma armature railgun that would eventually have a power injector added. Its purpose would then be to accelerate the powder to a very high rate of speed. A diagram of the BTR follows.

Figure 36: Geometry of the gun rails and the diagnostic coil.

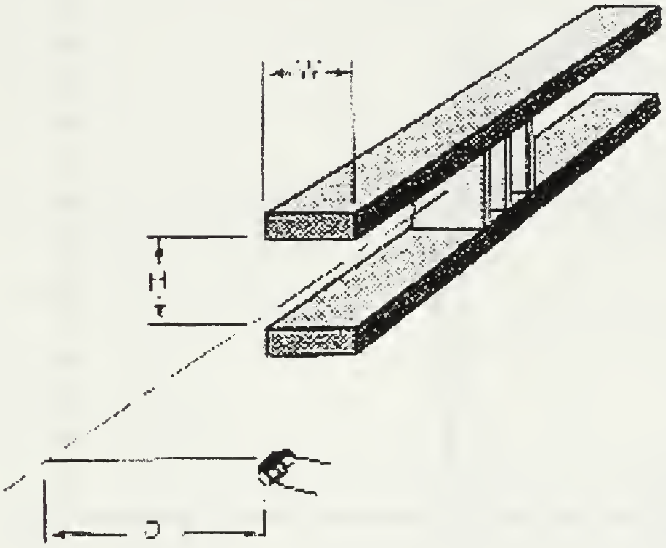

A program was written where the plasma armature was divided into 10 discrete current sheets. The program then calculated the B-dot coil outputs based on the superposition of equations (112) and (113). The ten current sheets were also assumed to contain current in the following percentages from the front of the armature working to the rear: 50, 14, 8, 7, 6, 5, 4, 3, 2, and 1. A simulation based on the program follows.

Figure 37: Predicted B-dot voltage for the BTR tests.

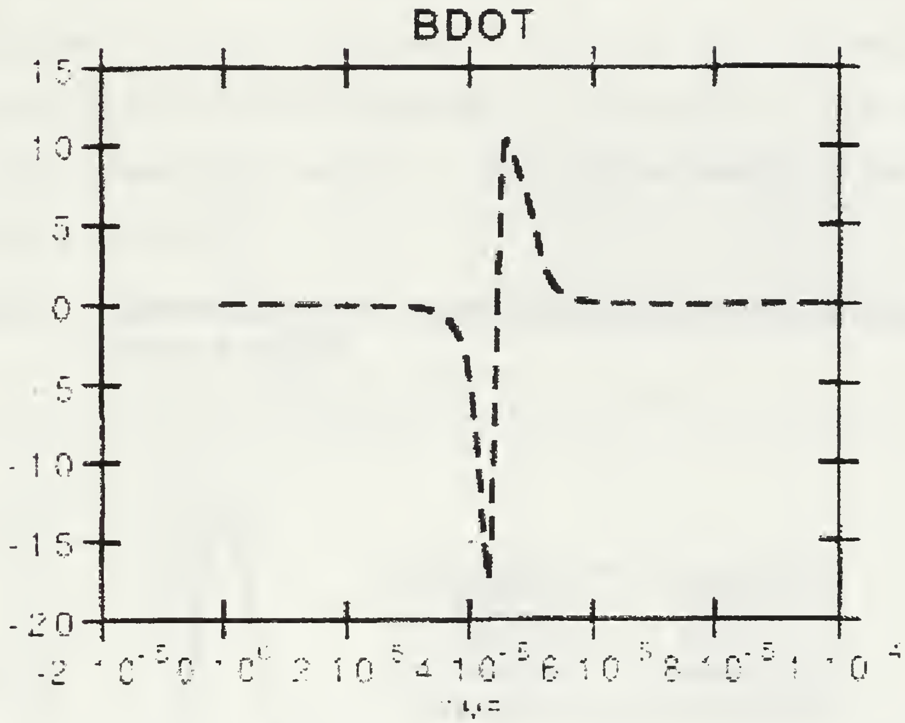

The B-dot coils in the bench test railgun had 30 turns and were wrapped on a 1.5 mm diameter form. The location of the coils were 0.5 in. from the centerline of the BTR that had a bore dimension of 0.5 in. by 0.5 in. (i.e. D = 0.5 in., W = 0.5 in., and H = 0.5 in.).

The output data shown from the program in figure (37) is found to be in good agreement with the actual data that was recorded during the BTR test series.

[illegible]

The result from the BTR experimental not only shows the accuracy of the simulation but also shows the consistency of the launcher. The data also shows that the armature is only affected by the parts of the rail in its immediate region. The experimental results follow (Zaworka).

Figure 38: Current waveforms for 10 shots using ceramic sidewalls and Inconel 718 rails in the BTR.

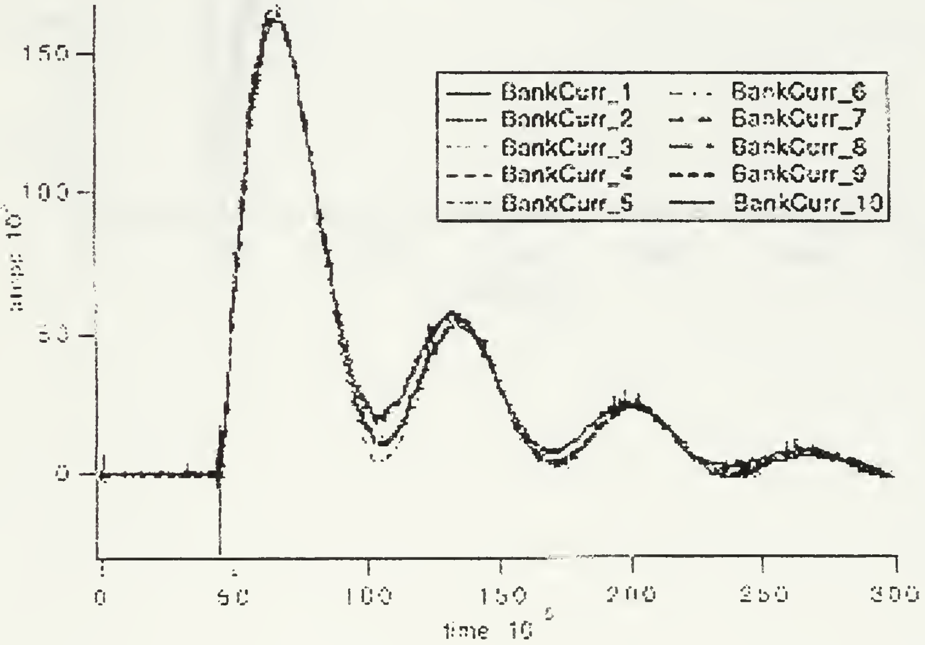

Figure 39: B-dot 1 waveforms for 10 shots using ceramic sidewalls and Inconel 718 rails in the BTR.

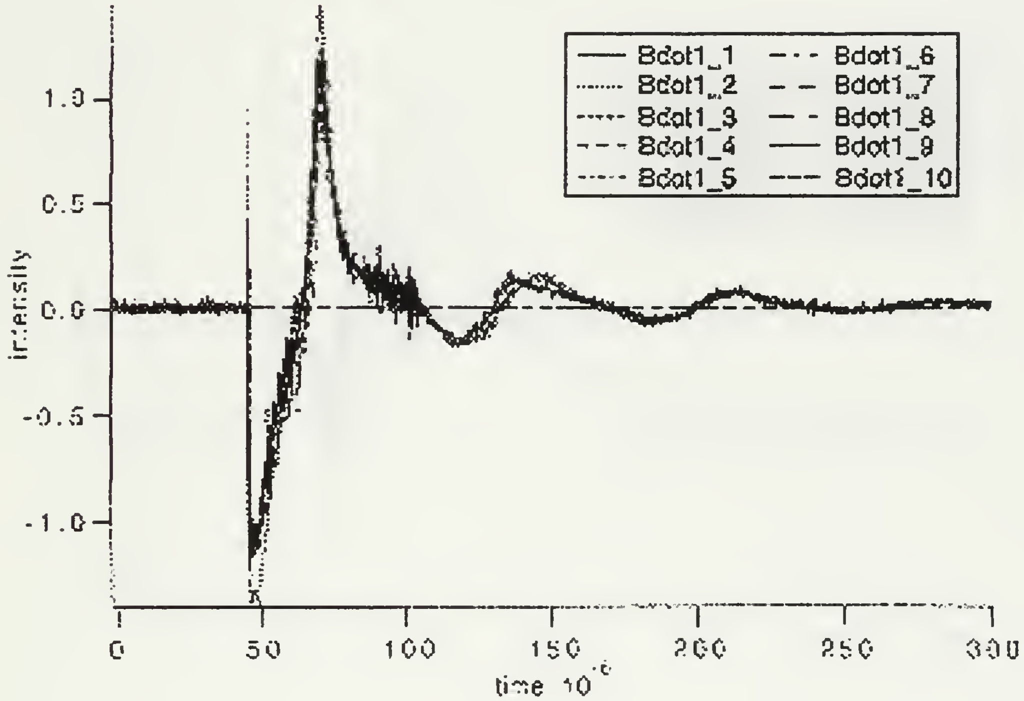

Figure 40: B-dot 2 waveforms for 10 shots using ceramic sidewalls and Inconel 718 rails in the BTR.

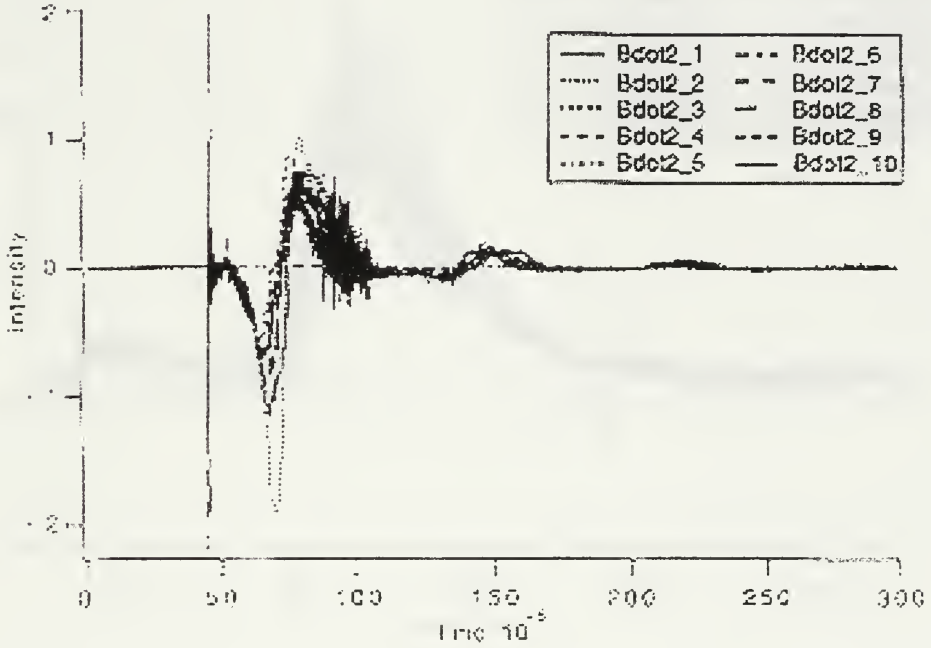

Figure 41: Pressure transducer #2 waveforms for ten shots using ceramic sidewalls and Inconel 718 rails in the BTR.

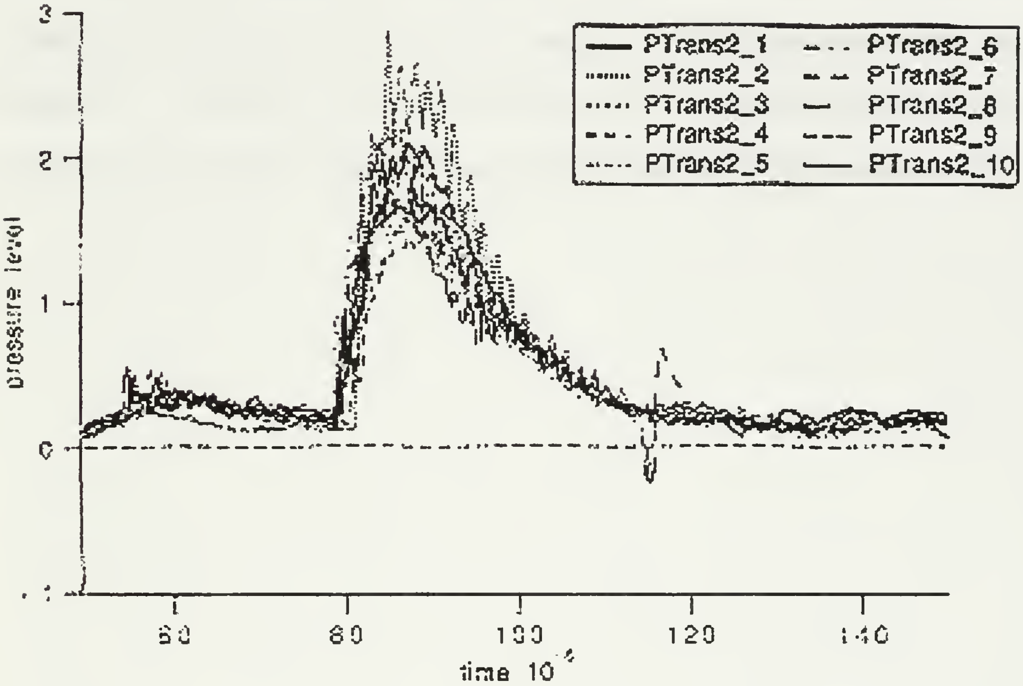

SECTION VI: CONCLUSIONS

The following section contains two chapters. Chapter 20 contains the overall conclusions of this paper. Chapter 21 consists of some thoughts to improve the design of some electromagnetic launchers.

Chapter 20: Overall Conclusions

In general, the paper shows that the electromagnetic launcher has the capacity to be used as an aircraft carrier catapult. Specifically, many items were discussed. First of all, this paper gives a comprehensive treatment to both railguns and coilguns for low and medium velocities. This includes an in-depth history of the aircraft catapult and also a study of the theory behind the electromagnetic launcher. Also, the limiting factors of such macroparticle accelerators were stressed for the specific application of aircraft launchers. The conditions imposed by aircraft launchers were then established. Through this discussion, it was established that the railgun would not be as effective as the coilgun for the purpose of aircraft launching. Finally, it was shown that the diagnostics of the electromagnetic launcher (e.g. position, velocity, and acceleration) are fundamental to the design process. The B-dot readings (i.e. dB/dt) were able to fully describe the final performance of an electromagnetic

launcher. With these tools and analysis, the design of an electromagnetic launcher can be accomplished to effectively launcher aircraft from the deck of an aircraft carrier.

Chapter 21: Thought for Improvements in Electromagnetic Launchers

After reviewing previously designed aircraft catapults, the theory of electromagnetic launchers, the power systems for EML, and an electromagnetic gun experiment, many things can be concluded. In particular, these conclusions can be drawn when the newest design of an electromagnetic aircraft launcher is taken into account.

The first conclusion is that aircraft launching technology has had to continue to evolve as the aircraft have evolved. It is also obvious that while naval aviation has grow by leaps and bounds in the past four decades, the launching technology has not changed much from the 1950's steam catapult. Another conclusion that can be drawn is that the theory of electromagnetic launchers has been sufficiently developed so as to meet the needs of an aircraft catapult. As a matter of fact, the theory shows that a very efficient catapult can be built without testing the limits of electromagnetic launchers. Finally, the most important conclusion is that it is possible to design and build an electromagnetic aircraft launcher.

Unfortunately, while there are many positives to the use of electromagnetic aircraft launchers, there are a few drawbacks to their implementation.

One of the biggest concerns is the power system for the launcher. In Kaman's design, the power system consisted of four disk alternators and a cycloconverter. While the cycloconverter appears to be able to perform its task, the disk alternators are the cause for some concern. First of all, the disk alternators are large rotating machines that would have to operate at very high speeds (6400 rpm). In a laboratory, high-speed rotating machines perform well where their fragile nature will not be affected. On an aircraft carrier with high winds and rough seas, the disk alternators could experience enough jarring to not only reduce their efficiency but also to possibly cease operation.

Another of the concerns for an electromagnetically powered aircraft launcher is electromagnetic interference. In order to store the energy required for a launch, the disk alternators must operate at very high frequencies (~2100 Hz). With high frequencies can come unwanted electrical

signals. While electromagnetic interference is normally undesired, it should be remembered that the aircraft catapult must launch aircraft that depend on electrically equipment for every phase of its operation.

The largest concern when designing a new system is its efficiency. While almost any new design would be more efficient than the existing steam catapults (~4-6%), the electromagnetic launcher from Kaman Electromagnetics (~70% efficient) does not meet the optimal efficiency allowable by the theory.

There are areas for improvement, and ways of achieving this improvement must be found. One of the more obvious ways to improve the electromagnetic launcher is to reduce the frequency. By doing this, any potential problems from electromagnetic interference can been decreased. One of the more obvious ways to reduce the require frequency is shown in the following equation:

$$v = 2\tau f$$

In the equation above, it is shown that the velocity is equal to twice the frequency and the pole

pitch. The pole pitch is the length of the windings in a particular pole. In Kaman's design, the pole pitch was a constant 8 mm though the entire length of the launcher. Therefore, the frequency was the only variable factor in the velocity. Conversely in the design by CEM-UT, the pole pitch was varied in five distinct steps. This means that the frequency in each of the steps need not be as high to achieve a similar velocity.

Therefore, it would seem that dividing the length of the launcher into five regions of increasing pole pitch would reduce the need for as high of a frequency. Also, by using a power source with an increasing frequency along with the increasing pole pitch, the efficiency can be greatly increased. So by decreasing the frequency, benefits in efficiency and reduced electromagnetic interference can be achieved. The one drawback to the increasing pole pitches is it will make the coils segments less modular (i.e. instead of one size, there will now be five sizes).

With some benefits reached, the very important problem of stability must be addressed. In the Kaman model, the power system is based on the performance of

four disk alternators. The disk alternators are high-speed rotary machines used to store a massive amount of energy (~ 121 MJ). The pulse forming networks provide a more stable alternative. The chances of a breakdown are less likely with the capacitor banks of a pulse forming networks than the high-speed rotors of the disk alternators. However, it should be noted that the energy density of the disk alternator is much higher than that of the pulse forming network (disk alternators ~ 18 MJ; capacitor banks in the pulse forming networks ~1.3 MJ). While the size of the pulse forming network can present a problem, it is a small price to pay for stability.

It can be concluded that by utilizing a pulse forming network and the increasing pole pitch sizes, the electromagnetic launcher can provide a feasible alternative to the current steam catapult. Not only can the electromagnetic launcher provide an efficient means to launch aircraft from the decks of aircraft carriers, but they can also do so with a high degree of reliability and safety.

APPENDIX A: CVX REQUIREMENTS FOR THE 21ST CENTURY

MISSION NEED STATEMENT FOR A 21ST CENTURY TACTICAL AVIATION SEA-BASED PLATFORM (U)

1. (U) DEFENSE PLANNING GUIDANCE ELEMENT

a. (U) This Mission Need Statement (MNS) provides requirements for tactical aviation (TACAIR) sea-based platforms for the 21st century. It addresses the Department of Defense "Defense Planning Guidance, FY-1997-2001," dated 9 May 1995, requiring the United States to:
(U) "... require the best equipped, best trained and best prepared military forces..." (p.1)
(U) "The primary mission of United States military forces has always been, and will continue to be, to protect the nation from direct threats and to deter, and, if necessary, fight and win the nation's wars.... deter and, if required decisively defeat aggression by projecting and sustaining U.S. power in two nearly simultaneous major regional conflicts (MRC);... Some U.S. forces must be forward-deployed or stationed in key overseas regions in peacetime... This demands highly qualified and motivated people, modern, well maintained equipment, viable joint doctrine, realistic training, strategic mobility and sufficient support and sustainment capabilities." (p.4&5)

PARAGRAPH ON FORCE STRUCTURE REMOVED

b. (U) This MNS should guide the 21st century TACAIR sea-based platform design, research, development and acquisition program decisions, service and joint doctrine, and cooperative efforts with U.S. allies.

2. (U) MISSION AND THREAT ANALYSIS

a. (U) Mission. The general missions of TACAIR sea-based platforms are to:
(1) (U) provide credible, sustainable, independent forward presence during peace time without access to land bases,
(2) (U) operate as the cornerstone of a joint and/or allied maritime expeditionary force in response to crises, and
(3) (U) carry the war to the enemy through joint multi-mission offensive operations by;
(a) (U) being able to operate and support aircraft in attacks on enemy forces ashore, afloat, or submerged independent of forward-base land facilities,
(b) (U) protecting friendly forces from enemy attack, through the establishment and maintenance of battlespace dominance independent of forward-based land facilities, and
(c) (U) engaging in sustained operations in support of the United States and its Allies independent of forward-based land facilities.
b. (U) Capabilities. The primary function of the 21st century TACAIR sea-based platform is to shelter, transport, launch, recover and maintain multi-mission tactical aircraft and tactical airborne systems suitable for sea-based operations. The core capabilities required for this platform to perform the above missions include:
(1) (U) strategic mobility - it must have the ability to independently deploy/respond quickly and operate with sufficient tactical flexibility, whenever and wherever required, to enable joint maritime expeditionary force operations.
(2) (U) sustainability - it must have the capacity to sustain itself, its aircraft and escort for extended periods without access to shore facilities.

(3) (U) survivability - it must be able to operate aircraft in hostile environments, protect itself from attack by threat weapons, and if hit, degrade gracefully and survive.
(4) (U) ability to deliver precise, high-volume firepower - it must be able to operate sufficient numbers of tactical aircraft, and carry sufficient ordnance and fuel to conduct simultaneous power projection, battle space dominance and surveillance operations for extended periods. It must provide tactical air support to the Joint Force Commander.
(5) (U) joint command and control - it must be interoperable and its communications suite must be fully compatible with other naval, expeditionary, interagency, joint, and allied forces. In addition, it must be able to operate as a Command and Control center, integrate information to develop a coherent tactical picture to support Joint Force, Battle Force, Battle Group and Air Wing planning, coordinate actions with other forces, and communicate the force's actions to appropriate commanders. The platform must have the capability to fully support a Joint Force Commander (JFC) and under limited circumstances be able to host an embarked JFC. Connectivity must include seamless integration of both organic and off-ship sensor inputs for power projection actions.
(6) (U) flexibility and growth potential - it must have the versatility to support current and future sea-based aircraft. It must have the ability to perform simultaneous multi-mission taskings and readily adapt to changing operational needs. In addition, it must have the flexibility to adapt to changes in future threats, missions and technologies.
c. (U) Threat.

PARAGRAPH REMOVED

d. (U) Shortfalls of Existing Systems

PARAGRAPH REMOVED

(1) (U) maintain required force levels for forward presence, crisis response and warfighting,
(2) (U) maintain an effective industrial base to assure continued support for sea-basing, and
(3) (U) take advantage of new technologies and design concepts that offer opportunities to develop sea-based platforms that are as capable, but more affordable than current platforms.

3. (U) NON-MATERIAL ALTERNATIVES

(U) Changes in doctrine, operational concepts, tactics, organization and training are not sufficient to address the issue of maintaining an affordable and capable sea-based aviation capability.
a. (U) U.S. or Allied doctrine: Doctrine changes required without a 21st century TACAIR sea-based platform would include: Acceptance of a decrease ability to deter/contain regional crises; inability to project expeditionary force strike power from the sea; severely degraded ability to project precise strike power against land targets; and, inability to maintain meaningful, visible forward presence for coalition building which is "independent" of host nation support and operational
approval.
b. (U) Operational concepts: A 21st century TACAIR sea-based platform optimized to leverage technology to perform multiple roles in both open ocean and littoral/enabling warfare environments, will be needed to execute the operational concepts contained in the Joint Maritime Strategy.
c. (U) Tactics: Tactics calling for the application of sea-based forces into the littorals, enabling follow-on forces as well as influencing nearby events, will place all naval forces at higher risk as

technological development and proliferation of adversaries' offensive systems grow. The TACAIR sea-based platform will aid measurably in the protection of those naval forces, but will need the enhanced self-protection systems to balance that growing threat. Simple changes in tactics would not provide the commensurate degree of protection that would be the result of building a new platform with greater self-protection areas of hull and bottom defense.

d. (U) Organization: Organizational changes, such as increased forward basing and/or double crewing of carries, in lieu of procurement were determined to be infeasible. Acceptance of these alternatives may provide insufficient assets for crisis response or joint warfighting in a single or two nearly simultaneous MRC contingency.

e. (U) Training: Training alternatives offering the potential to maintain force capability in a smaller force manned with fewer personnel rely heavily on holistic, embedded training. This training capability must be an integral part of the total ship architecture called out as a mission need in the 21st century carrier. Future aircraft carriers must be ready to fight simultaneous multi-warfare engagements in littoral warfare that will proceed so rapidly that crew response times will be critical. Although improvements in embedded training and changes in training concepts will mitigate to a degree the increased threat, they will be insufficient in themselves without the benefit of survivability and defensive systems improvements.

4. (U) POTENTIAL MATERIAL ALTERNATIVES

a. (U) Alternative design concepts include:
(1) (U) new ship designs, which may include nuclear or non-nuclear propulsion or advanced/unconventional hull forms
(2) (U) a modified repeat Nimitz class carrier
(3) (U) Mobile Offshore Basing (MOB) Concepts

b. (U) The ongoing Nimitz class acquisition program could potentially address this need through a mod repeat program by capitalizing on advanced technology. However, to do this, it would need to employ a significantly different architectural approach in the design.

c. (U) As part of their shipbuilding programs, various Allies have combat, hull, mechanical and electrical system programs ongoing of under development that offer possible cooperative opportunities. These subsystem designs will be examined. All meaningful cooperative opportunities can be realized without a formal cooperative development program for a 21st century TACAIR sea-based platform.

5. CONSTRAINTS

a. (U) Key Boundary Conditions.

(1) (U) Architecture. The ship design must employ a total ship, aircraft and weapons system architecture/engineering approach that optimizes life cycle cost and performance; permits rapid upgrade and change in response to evolving operational requirements; allows computational and communications resources to keep technological pace with commercial capabilities and allows for full realization of the command, control, communications, computers, and intelligence (C4I) for the warrior (C4IFTW) concept; and provides the capability to survive and fight hurt. More specifically this implies physical element modularity; functional sharing of hardware (across all services); open systems information architecture; ship wide resource management; automation of Command, Control, Communications, and Computers (C4I), combat, aircraft support, ordnance handling, management; automation and minimization of maintenance and administrative functions; integrated systems security; and embedded training. The approach should also promote commonality with other ship designs.

(2) (U) Design. Consideration should be given to the maximum use of modular construction design in the platforms infrastructure. Emerging technologies must be accounted for during the developmental phase. Modern, flexible information processing must be built into any new weapons system. Since communication and data systems hold the greatest potential for growth, and therefore obsolescence, their installations must be modularized as much as possible to allow for future upgrades. The inherent vulnerabilities of communications and data systems requires information systems security to be engineered into the design. Use standard man-to-machine interfaces among the systems onboard. The man-to-machine interfaces should be consistent with existing user friendly systems. This capability must comply with applicable information technology standards contained the Technical Architecture Framework for Information Management (TAFIM), Volume 7, Adopted Information Technology Standards (AITS).

(3) (U) Personnel. The platform should be automated to a sufficient degree to realize significant manpower reductions in engineering, damage control, combat systems, ship support and Condition III watchstanding requirements. Reduced manning concepts used by other Navies should be reviewed to leverage advanced technologies and future advanced technology concepts in an effort to minimize shipboard manning requirements. Preventive maintenance manpower requirements must be reduced by incorporating self-analysis features in equipment designs, and by selecting materials and preservatives which minimize corrosion. Manpower, Personnel and Training (MPT) analysis will be performed in accordance with OPNAVINST 5311.7 (HARDMAN). This analysis will recommend options to exploit the use of technology to reduce MPT requirements. Trade-offs which reduce MPT requirements will be favored during design and development. Final MPT determination will be documented and validated in a Navy Training Plan in accordance with OPNAVINST 1500.8.

(4) (U) Backfit. Major functional elements of a 21st century TACAIR sea-based platform must be applicable to other forward fit ship construction programs. Consideration must also be given to the ability to retrofit into existing carrier classes; however, this must not be done at the expense of achieving performance in new construction.

b. Operational Constraints

(1) (U) The 21st century TACAIR sea-based platform must remain fully functional and operational in all environments regardless of time of day, whether conducting independent of force operations, in heavy weather or in the presence of electromagnetic, nuclear, biological and chemical contamination and/or shock effects from nuclear and conventional weapon attack.

(2) (U) Any 21st century TACAIR sea-based platform must meet the survivability requirements of Level III as defined in OPNAVINST 9070.1. Topside systems components shall be decontaminated through use of a countermeasure wash down system and portable Decontamination (DECON) methods.

(3) (U) The 21st century TACAIR sea-based platform must provide landing and hangar facilities, and ammunition storage for operational support of required aviation assets.

(4) (U) The platform must be able to operate in U.S., foreign, and international waters in full compliance with existing U.S. and international pollution control laws and regulations.

(5) (U) All ship and combat system elements must make use of standard subsystems and meet required development practices. The 21st century TACAIR sea-based platform must be fully integrated with other U.S. Navy, Marine Corps, joint and allied forces, and other agencies (e.g., Theater Air Defense Architecture) in combined, coordinated operations. For example, linkage with standard data bases from the Defense Mapping Agency (DMA) will minimize ancillary costs and promote maximum interoperability with the widest number of weapons and sensor systems. Joint goals for standardization and interoperability will be achieved to the maximum feasible extent.

(6) (U) The platform must be able to embark Special Operations Forces (SOF) and Joint Forces when required for selected missions.

6. (U) JOINT POTENTIAL DESIGNATOR (JPD)

(U) JPD overall is TBD. Service assessments are as follows:

a. (U) USA. Recommend JPD of Joint Interest based on the interoperability requirements implied in paragraphs 2.b.(1) and (5) and 5.b.(5).
b. (U) USAF. Recommended Joint Potential Designator for this MNS is "Joint Interest" due to the need to be fully interoperable with other services' Battle Management/C4I systems.
c. (U) USMC. No comment.

(This following report is located at the Team CVX web site.)

REFERENCES

Abramowitz, G. and A. Stegun. Handbook of Mathematical Functions. Dover Publications, New York, 1965.

Aichholzer, G., C. Tauschitz, and H. Kofler. “Limits of Coil Launcher Systems.” Proceeding of the 5th Symposium on Electromagnetic Launch Technology, Sandestin, Florida, April 2-5, 1990.

Augsburger, B., et al. “DRA 500 kJ multi-module capacitor bank.” IEEE Transactions on Magnetics, Vol. 31, January 1995.

Boldea, I., and S. A. Nasar. Linear Motion Electromagnetic Systems. John Wiley & Sons, New York, 1985.

Bondaletov, V. N., et al. “Efficiency of Conductor Acceleration in the Pulsed Magnetic Field of a Solenoid.” Soviet Journal of Applications in Mechanical and Technogical Physics, Vol. 24, No. 2, March-April 1983: 210-215.

Calvin, Hugh A., and Steve P. Virostek. “Railgun Electromagnetism.” IEEE Transactions on Magnetics, Vol. 31, No. 1, January 1995: 107-112.

Di Capua, M. and H. L. Kurtz. “Electrolytic Capacitor Power Source Design for Quasi-Steady Magnetoplasmadynamic Arcs.” J. Spacecraft, August 1974.

Driga, M. D., W. F. Weldon, and H. H. Woodson. "Electromagnetic Induction Launchers." IEEE Transactions on Magnetics, Vol. MAG-22, No. 6, November 1986: 1453-1458.

Doyle, Michael R., et al. "Electromagnetic Aircraft Launch System-EMALS." IEEE Transactions on Magnetics, Vol. 31, No. 1, January 1995: 528-533.

Esposito, N., A. Musolino, and M. Raugi. "Modeling of Three-Dimensional Nonlinear Eddy Current Problems with Conductors in Motion by an Integral Formulation." IEEE Transactions on Magnetics, Vol. 32, No. 3, May 1996.

Glasoe, G. N. and J. V. Lebacqz. Pulse Generators. McGraw-Hill, New York, 1948.

Grover,F. W. Inductance Calculations, Working Formulas and Tables. Dover Publishing, New York, 1946.

Guillemin, E. A. Synthesis of Passive Networks. John Wiley & Sons, New York, 1957.

Jablonski, E. Man with Wings: A Pictorial History of Aviation. Doubleday and Company, Garden City, New York, 1980.

Jamison, K. A., M. Marquez-Reines, and H.S. Burden. “Measurements of Spatial Distribution of Current in a Railgun Arc Armature.” IEEE Transactions on Magnetics, Vol. MAG-20, March 1984.

Kolm, Henry, and Peter Mongeau. “Basic Principles of Coaxial Launch Technology.” IEEE Transactions on Magnetics, Vol. 12, No. 2, March 1984: 227-230.

Koops, Marcel, and Arnold Schoolderman. “Scaling Relations for Electromagnetic Launch Processes.” 9th EML Conference, Edinburg, Scotland, May 12-15, 1998.

Laithwaite,E. R. Propulsion without Wheels. The English University Press, Aylesbury, Bucks, England, 1970.

Levi, E., et al. “Guidelines for the Design of Synchronous-Type Coilguns.” Polytechnic University, Brooklyn, New York.

Lu, X. N., et al. “Transition Between Two Sections in a Linear Induction Launcher (LIL).” IEEE Transactions on Magnetics, Vol. 31, No. 1, January 1995: 493-498.

McKinney, K. and P. Mongeau. “Multiple Stage Pulsed Induction Acceleration.” IEEE Transactions on Magnetics, Vol. MAG-20, No. 2, March 1984.

McNab, Ian R. “Pulsed Power for Electric Guns.” IEEE Transactions on Magnetics, Vol. 33, No. 1, January 1997: 453-459.

McNab, I. R., F. LeVine, and M. Aponte. "Experiments with the Green Farm Electric Gun Facility." IEEE Transactions on Magnetics, Vol. 31, January 1995.

Miller, Nathan The U.S. Navy: A History. William Morrow, New York, 1990.

Musolino, A., M. Raugi, and B. Tellini. "3-D Field Analysis in Tubular Induction Launchers with Armature Transverse Motion." Department of Electrical Systems and Automation, University of Pisa, 1998.

Musolino, Antonino, Marco Raugi, and Bernardo Tellini. "Pulse Forming Network Optimal Design for the Power Supply of Eml Launchers." IEEE Transactions on Magnetics, Vol. 33, No. 1, January 1997: 480-483.

Navy Lakehurst Web Site. "Why Naval Aviation is Unique." `www.lakehurst.navy.mil/pic25.gif`, March 30, 1998.

Parker, Jerald. "Magnetic-Probe Diagnostics for Railgun Plasma Armatures." IEEE Transactions on Plasma Science, Vol. 17, No. 3, June 1989: 487-500.

Shokair, I. R. "Projectile Transverse Motion and Stability in Electromagnetic Induction Launchers." IEEE Transactions on Magnetics, Vol. 31, No. 1, January 1995.

Skerrett, R. G. "Catapulting a Hydro-Aeroplane from a Fighting Ship." Scientific American, December 14, 1912: 512.

Team CVX. "Mission Need Statement for a 21st Century Tactical Aviation Sea-based Platform." `www.navsea.navy.mil/cvx/teamcvx.html`, February 1997.

"The Catapult Museum." State of the Technology Arts and Communication, `www.nzp.com/1000airplane.html`, Marion County, California, 1995.

The Steam Catapult. Department of the Navy, United States Government Printing Office, 1957.

Wang, De-man, et al. "The Magnetic Leviation of the Projectile in Coilguns." IEEE Transactions on Magnetics, Vol. 33, No. 1, January 1997: 195-200.

Weldon, W. F., M. D. Driga, H. H. Woodson, and J. H. Gully. "Technical Proposal for the Development and Test of a Prototype, Subscale, Nimitz-Class Electromagnetic Aircraft Launcher(Catapult)." Center for Electromechanics, University of Texas at Austin, September 1985.

Williamson, Stephen, and Alexander Smith. "Pulsed Coilgun Limits." IEEE Transactions on Magnetics, Vol. 32, No. 1, January 1997: 201-207.

Williamson, S., and J. R. Smith. "Application of Minimization Algorithms in Electrical Engineering," IEEE Proceedings Part B, 127(8), November 1980.

Zabar, Z., X.N. Lu, J.L. He, L. Birenhaum, and E. Levi, "A 500 m/s Linear Induction Launcher," Proceedings IEEE 8th Pulsed Power Conference, San Diego, CA; June 17-19, 1991.

Zaworka, Ray. Personal Interview. 25 April 1998.

Vita

Aaron Michael Still was born in Dunedin, Florida on November 26, 1973. He is the son of Michael William and Barbara Lucinda Still. After graduating from Lancaster High School in Lancaster, Texas in 1992, he attended the United States Naval Academy. He graduated with merit from the Naval Academy on May 24, 1996 with a Bachelor of Science in Systems Engineering. On the same day, he was commissioned as an Ensign in the United States Navy Civil Engineer Corps. In August 1996, he began graduate study in electrical engineering at the University of Texas at Austin.

Permanent address: 933 Francis Street
Lancaster, Texas 75146

This thesis was typed by the author.

20 5INPS Tn 1746
1/99 22527-157
ICI INFORMATION CONSERVATION INC

DUDLEY KNOX LIBRARY

3 2768 00360578 3